A THIN RIVULET OF PERFECTLY WETTING FLUID SUBJECT TO A LONGITUDINAL SURFACE SHEAR STRESS

by J. M. SULLIVAN, S. K. WILSON *and* B. R. DUFFY

(*Department of Mathematics, University of Strathclyde,*
Livingstone Tower, 26 Richmond Street,
Glasgow G1 1XH, United Kingdom)

[Received 26th January 2007. Revise 7th September and 11th October 2007]

Summary

The lubrication approximation is used to obtain a complete description of the steady unidirectional flow of a thin rivulet of perfectly wetting fluid on an inclined substrate subject to a prescribed uniform longitudinal surface shear stress. The quasi-steady stability of such a rivulet is analysed, and the conditions under which it is energetically favourable for such a rivulet to split into one or more subrivulets are determined.

1. Introduction

There are many practically important situations in which an external airflow has a significant effect on the behaviour of a film of fluid, and consequently a considerable amount of theoretical and numerical work has been undertaken in order to understand the flows that can occur. Examples include the work by King and Tuck (**1**) and King, Tuck and Vanden-Broeck (**2**) on a thin film and a droplet, respectively, on an inclined substrate supported against gravity by an upward airflow, and the work by Tsao, Rothmayer and Ruban (**3**) on the stability of thin films on airfoils in the presence of an airflow. Other examples include the work by Kriegsmann, Miksis and Vanden-Broeck (**4**) on the effect of a steadily moving pressure disturbance on a thin film on an inclined substrate, the work by Myers and Thompson (**5**) on a thin film on an inclined substrate in the presence of an airflow, the work by McKinley, Wilson and Duffy (**6**) and McKinley and Wilson (**7**, **8**) on a thin ridge and a thin droplet subject to a jet of air, and the work by Villegas-Díaz, Power and Riley (**9**) on a thin film on a horizontal cylinder subject to a uniform azimuthal surface shear stress due to an airflow.

The flow and, in particular, the break-up of a film or a rivulet on a substrate has been considered by several authors. Hartley and Murgatroyd (**10**) obtained two different criteria for the break-up of a film on a vertical substrate, namely a force-balance criterion at the upstream stagnation point of a dry patch and a minimum rate-of-energy-flow criterion. They used each criterion to calculate when it is favourable for a film driven purely by gravity and a film driven purely by a prescribed uniform longitudinal surface shear stress due to an external airflow to break up into rivulets. Hobler (**11**) used a minimum energy criterion to calculate when it is energetically favourable for a film on a vertical substrate to break up into rivulets. Bankoff (**12**) considered the flow of a film and of a periodic array of contiguous identical rivulets on a vertical substrate, and compared the energies of the two configurations

to determine when it is energetically favourable for the film to break up into the rivulets. However, Mikielewicz and Moszynski (**13**) showed that it is necessary to consider an array of rivulets with dry substrate between them in order to obtain physically meaningful results (and, in particular, showed that if an algebraic error in Bankoff's calculation is corrected then his analysis yields unphysical results). Subsequently Mikielewicz and Moszynski (**14**) improved their earlier analysis (**13**) by using a conformal mapping technique to obtain the exact (rather than an approximate) solution for the velocity distribution of a rivulet, and also applied their method to flow driven purely by a prescribed uniform longitudinal surface shear stress. Schmuki and Laso (**15**) calculated approximately when it is energetically favourable for a rivulet on an inclined substrate to break up into several smaller subrivulets in an unsteady manner which they termed "oscillating" or "pendulum" rivulets. El-Genk and Saber (**16**) used numerically calculated solutions for the velocity distribution of a rivulet to calculate when it is energetically favourable for a film on a vertical substrate to break up into rivulets. Subsequently Saber and El-Genk (**17**) extended their earlier work (**16**) to determine when it is energetically favourable for a film on an inclined substrate subject to a prescribed non-uniform longitudinal surface shear stress to break up into rivulets. In both works the validity of their calculations was demonstrated by comparison with experimental results. The flow of a rivulet on an inclined substrate subject to a prescribed uniform longitudinal surface shear stress was investigated by Myers, Liang and Wetton (**18**) who solved the problem numerically and asymptotically for a thin rivulet, and found that the asymptotic solution is in good agreement with the numerical solution for values of the contact angle up to about 30°. Myers et al. (**18**) also calculated when it is energetically favourable for a purely gravity-driven rivulet to split into two subrivulets, and conjectured that it is never energetically favourable for a purely shear-driven rivulet to split in the same manner. The flow of a thin rivulet on a vertical substrate subject to a prescribed uniform longitudinal surface shear stress was considered by Wilson and Duffy (**19**) who determined when it is energetically favourable for such a rivulet to split into two subrivulets. In particular, they showed that it can be energetically favourable for a purely shear-driven rivulet to split into two subrivulets (i.e. that the conjecture of Myers et al. (**18**) is false).

One context in which these ideas may have practical application is the intriguing problem of the so-called Rain-Wind Induced Vibrations (RWIVs) of the cables of cable-stayed bridges such as the Erasmus Bridge in Rotterdam. RWIVs have been the subject of extensive study in recent years, much of it dating back to the pioneering work by Hikami and Shiraishi (**20**). An interaction between the wind and the rivulets of rainwater on the cables can induce vibrations of the cables which can be severe enough to cause significant damage to the bridge. For example, RWIVs were the subject of a numerical study by Geurts, Vrouwenvelder, van Staalduinen and Reusink (**21**), and analytical work has been carried out by Xu and Wang (**22**) (who considered both a horizontal cable with a fixed rivulet, and an inclined cable with a moving rivulet) and by Lemaitre, Mahmud Alam, Hémon, de Langre and Zhou (**23**) (who developed a model for the response of a film of rainwater on a cable under the action of the wind).

All of the work on rivulets described above concerns non-perfectly wetting fluid (i.e. fluid with a non-zero contact angle at its contact lines). There has been far less work on rivulets of perfectly wetting fluid (i.e. fluid with zero contact angle at its contact lines). Kuibin (**24**) and Alekseenko, Geshev and Kuibin (**25**) considered a thin rivulet on the underside of an inclined circular pipe. In particular, Kuibin (**24**) obtained the leading-order asymptotic

solution for a thin and narrow rivulet on the underside of an inclined locally parabolic substrate. Wilson and Duffy (**26**) investigated the general problem of a thin rivulet on a transversely non-uniform inclined substrate. Recent work by the same authors (**27**) determined when it is energetically favourable for such a rivulet on a uniform inclined substrate to split into two or more subrivulets. None of these studies considered the effect of an external airflow on the rivulet.

In the present paper we use the lubrication approximation to obtain a complete description of the steady unidirectional flow of a thin rivulet of perfectly wetting fluid on an inclined substrate subject to a prescribed uniform longitudinal surface shear stress. We analyse the quasi-steady stability of such a rivulet, and determine the conditions under which it is energetically favourable for such a rivulet to split into one or more subrivulets.

2. Problem Set-Up

Consider the steady unidirectional flow of a thin rivulet on a planar substrate inclined at an angle α to the horizontal with constant semiwidth a and constant volume flux Q subject to a prescribed uniform longitudinal surface shear stress τ. Cartesian axes $Oxyz$ are chosen with the x-axis down the slope, the y-axis parallel to the substrate, and the z-axis normal to the substrate. The fluid is assumed to be Newtonian with constant density ρ, viscosity μ, and surface tension γ. The velocity $\mathbf{u} = u(y,z)\mathbf{i}$ and pressure $p = p(x,y,z)$ of the fluid are governed by the familiar mass-conservation and Navier–Stokes equations subject to the usual normal and tangential stress balances and the kinematic condition at the free surface $z = h(y)$, and no slip at the substrate $z = 0$. By definition the rivulet has zero thickness at its contact lines $y = \pm a$, i.e. $h(\pm a) = 0$, and the contact angle θ is given by $\theta = \mp h'(\pm a)$, where the prime denotes differentiation with respect to argument. We are primarily concerned with steady flow of a perfectly wetting fluid for which the contact angle is zero, i.e. $\theta = 0$, as shown in Figure 1. However, the quasi-steady stability analysis described in Section 5 involves the unsteady evolution of a rivulet with non-zero contact angle, and with this in mind, it is appropriate to consider first the general case $\theta \neq 0$ before considering the special case $\theta = 0$.

We consider a thin rivulet with a small transverse aspect ratio $\epsilon \ll 1$; in this case it is appropriate to non-dimensionalise y and a with l, z and h with ϵl, u with $U = \rho g \epsilon^2 l^2/\mu$, Q with $\epsilon l^2 U = \rho g \epsilon^3 l^4/\mu$, $p - p_\infty$ with $\rho g \epsilon l$ and τ with $\rho g \epsilon l$, and scale θ with ϵ, where $l = (\gamma/\rho g)^{1/2}$ is the capillary length, g is acceleration due to gravity and p_∞ is the uniform atmospheric pressure. Since the flow is unidirectional, the mass-conservation equation and kinematic boundary condition are identically satisfied, and at leading order in ϵ the Navier–Stokes equation reduces to

$$0 = \sin\alpha + u_{zz}, \quad 0 = -p_y, \quad 0 = -p_z - \cos\alpha, \tag{2.1}$$

to be solved subject to boundary conditions of no slip at the substrate,

$$u = 0 \quad \text{on} \quad z = 0, \tag{2.2}$$

balances of normal and tangential stress at the free surface,

$$p = -h'' \quad \text{and} \quad u_z = \tau \quad \text{on} \quad z = h, \tag{2.3}$$

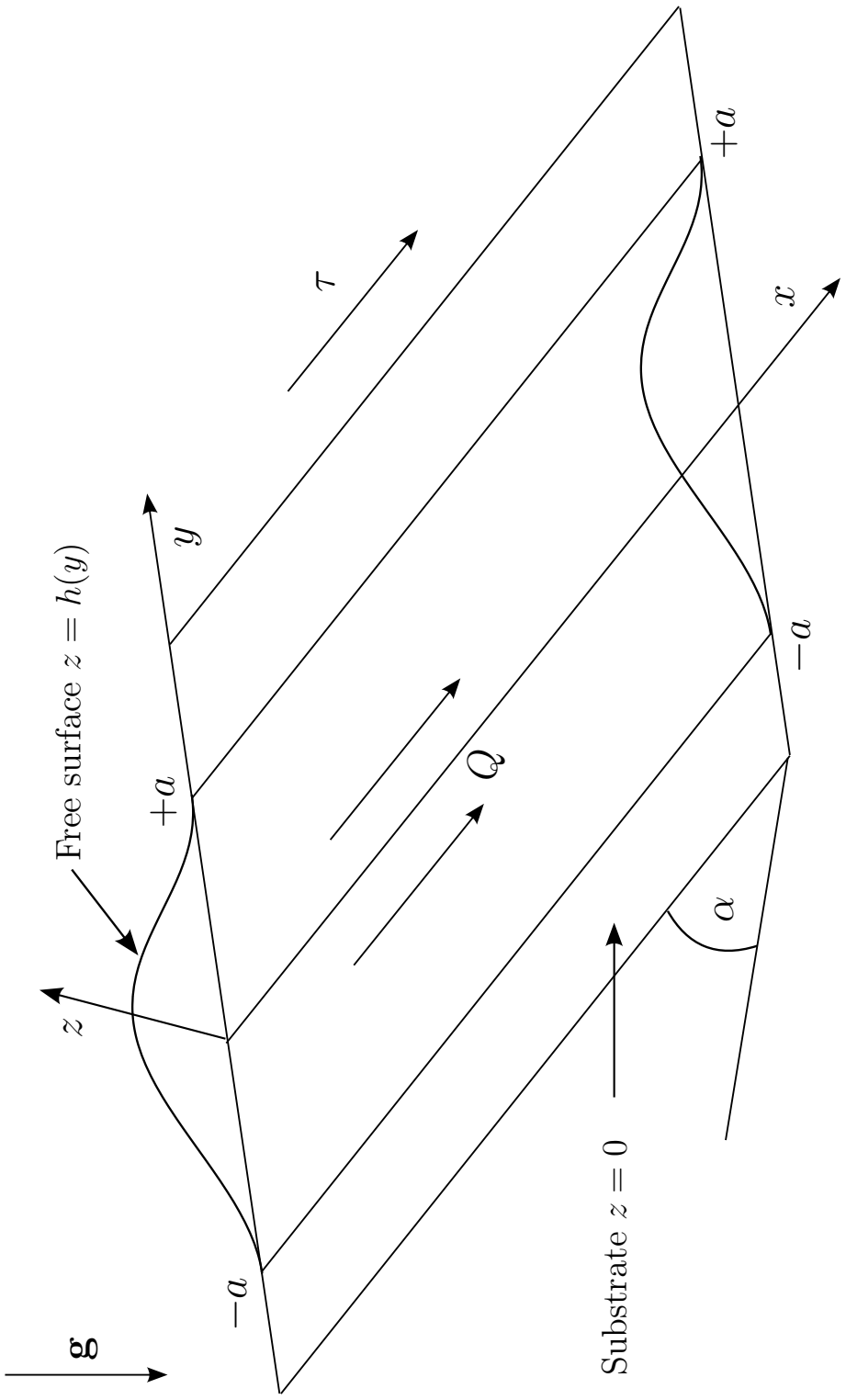

Fig. 1 Geometry of the problem.

and appropriate conditions at the contact lines, namely

$$h = 0 \quad \text{and} \quad h' = \mp\theta \quad \text{at} \quad y = \pm a. \tag{2.4}$$

Therefore we can readily obtain the solution

$$u = \frac{\sin\alpha}{2}(2h - z)z + \tau z, \tag{2.5}$$

$$p = (h - z)\cos\alpha - h''. \tag{2.6}$$

In particular, the free surface velocity $u_{\rm s} = u_{\rm s}(y) = u(y, h)$ is given by

$$u_{\rm s} = \frac{\sin\alpha}{2}h^2 + \tau h. \tag{2.7}$$

Substituting (2.6) into the second equation in (2.1) yields a third-order ordinary differential equation for the free surface profile h, namely

$$(h'' - \cos\alpha\, h)' = 0, \tag{2.8}$$

to be solved subject to (2.4). In the general case $\theta \neq 0$ we obtain

$$h = \theta \times \begin{cases} \dfrac{\cosh ma - \cosh my}{m\sinh ma} & \text{when} \quad 0 \leq \alpha < \dfrac{\pi}{2}, \\ \dfrac{a^2 - y^2}{2a} & \text{when} \quad \alpha = \dfrac{\pi}{2}, \\ \dfrac{\cos my - \cos ma}{m\sin ma} & \text{when} \quad \dfrac{\pi}{2} < \alpha \leq \pi, \end{cases} \tag{2.9}$$

where $m = \sqrt{|\cos\alpha|}$. In the special case $\theta = 0$ Wilson and Duffy (**26**) showed that when $0 \leq \alpha \leq \pi/2$ there are no solutions for h, but that when $\pi/2 < \alpha \leq \pi$ there is a simple solution corresponding to a pendent rivulet hanging underneath the substrate, namely

$$a = \frac{\pi}{m} \tag{2.10}$$

and

$$h = \frac{h_{\rm m}}{2}\left(1 + \cos my\right), \tag{2.11}$$

where $h_{\rm m} = h(0)$ is the (unknown) maximum height of the rivulet. As Wilson and Duffy (**26**) showed, when $\pi/2 < \alpha \leq \pi$ there are, in fact, infinitely many solutions, but since all the other solutions are simply appropriately re-scaled copies of (2.10) and (2.11) representing arrays of contiguous identical rivulets, we do not consider them any further here.

The local volume flux $\bar{u} = \bar{u}(y)$ is given by

$$\bar{u} = \int_0^h u\,{\rm d}z = \frac{\sin\alpha}{3}h^3 + \frac{\tau}{2}h^2, \tag{2.12}$$

and so the total volume flux down the rivulet Q is given by

$$Q = \int_{-a}^{+a} \bar{u}\, \mathrm{d}y = \frac{\sin\alpha}{3} \int_{-a}^{+a} h^3\, \mathrm{d}y + \frac{\tau}{2} \int_{-a}^{+a} h^2\, \mathrm{d}y. \tag{2.13}$$

In the general case $\theta \neq 0$ we obtain

$$Q = \frac{\theta^3 \sin\alpha}{9m^4} f(ma) + \frac{\theta^2 \tau}{2m^3} g(ma), \tag{2.14}$$

where the functions $f = f(ma)$ and $g = g(ma)$ (arising from the contributions due to gravity and surface shear stress effects, respectively) are given by

$$f(ma) = \begin{cases} 15ma\coth^3 ma - 15\coth^2 ma - 9ma\coth ma + 4 & \text{when} \quad 0 \leq \alpha < \dfrac{\pi}{2}, \\ \dfrac{12}{35}(ma)^4 & \text{when} \quad \alpha = \dfrac{\pi}{2}, \\ -15ma\cot^3 ma + 15\cot^2 ma - 9ma\cot ma + 4 & \text{when} \quad \dfrac{\pi}{2} < \alpha \leq \pi, \end{cases} \tag{2.15}$$

and

$$g(ma) = \begin{cases} 3ma\coth^2 ma - 3\coth ma - ma & \text{when} \quad 0 \leq \alpha < \dfrac{\pi}{2}, \\ \dfrac{4}{15}(ma)^3 & \text{when} \quad \alpha = \dfrac{\pi}{2}, \\ 3ma\cot^2 ma - 3\cot ma + ma & \text{when} \quad \dfrac{\pi}{2} < \alpha \leq \pi. \end{cases} \tag{2.16}$$

The corresponding results of Wilson and Duffy (**30**, **19**) are recovered in the special case $\tau = 0$ and in the limit $\alpha \to \pi/2^+$, respectively. In the special case $\theta = 0$ we obtain

$$Q = \frac{\pi}{24m} \left(5\sin\alpha\, h_{\mathrm{m}} + 9\tau\right) h_{\mathrm{m}}^2. \tag{2.17}$$

If the flux takes the prescribed value $Q = \bar{Q}$, then (2.14) determines the appropriate value(s) of a when $\theta \neq 0$ and (2.17) determines the appropriate value(s) of h_{m} when $\theta = 0$. Once a or h_{m} is known the rivulet solution given by (2.5), (2.6) and (2.9) (when $\theta \neq 0$) or (2.10) and (2.11) (when $\theta = 0$) is completely determined.

Henceforth (except for the quasi-steady stability analysis described in Section 5) we shall restrict our attention to the subject of this work, namely the steady flow of a rivulet of perfectly wetting fluid with $\theta = 0$.

In the special case of no prescribed shear stress, $\tau = 0$, the rivulet is purely gravity-driven and the equation $Q = \bar{Q}$ has the simple explicit solution obtained by Wilson and Duffy (**26**), namely

$$h_{\mathrm{m}} = \left(\frac{24\bar{Q}m}{5\pi\sin\alpha}\right)^{\frac{1}{3}}. \tag{2.18}$$

In the general case $\tau \neq 0$ the equation $Q = \bar{Q}$ may be written in the form

$$\left(\frac{h_{\mathrm{m}}\sin\alpha}{\tau}\right)^3 + \frac{9}{5}\left(\frac{h_{\mathrm{m}}\sin\alpha}{\tau}\right)^2 = \frac{24\bar{Q}m\sin^2\alpha}{5\pi\tau^3}, \tag{2.19}$$

showing that $h_{\mathrm{m}} \sin\alpha/\tau$ depends on the parameters $\bar{Q}$, α and τ only in the combination $\bar{Q}m\sin^2\alpha/\tau^3$ in a way that can be written down explicitly but which is rather unwieldy; see Appendix A. In particular, when $\tau < 0$ (but not when $\tau \geq 0$) there is always a non-trivial solution corresponding to a rivulet with zero net flux, $\bar{Q} = 0$, given by $h_{\mathrm{m}} = h_{\mathrm{m}0}$, where

$$h_{\mathrm{m}0} = -\frac{9\tau}{5\sin\alpha}. \tag{2.20}$$

In the limit of large positive or negative shear stress, $|\tau| \to \infty$, the effect of shear stress dominates the effect of gravity and so τ and $\bar{Q}$ must have the same sign, and at leading order in τ the rivulet is purely shear-driven and h_{m} is given explicitly by

$$h_{\mathrm{m}} = \left(\frac{8\bar{Q}m}{3\pi\tau}\right)^{\frac{1}{2}}. \tag{2.21}$$

In the limit of large positive flux, $\bar{Q} \to \infty$, the rivulet is deep (i.e. $h_{\mathrm{m}} \to \infty$), and the effect of gravity dominates the effect of shear stress, so that at leading order h_{m} is given by (2.18). In the limit of small flux, $\bar{Q} \to 0$, either the rivulet becomes shallow, and the effect of shear stress dominates the effect of gravity, so that at leading order h_{m} is given by (2.21), or, when $\tau < 0$, the effects of shear stress and gravity balance, so that the rivulet has finite height, given at leading order by (2.20).

3. Categorisation of Flow Patterns

All of the possible cross-sectional flow patterns that can occur may be categorised into five types which, following the notation introduced by Wilson and Duffy (**19**) for a rivulet of non-perfectly wetting fluid on a vertical substrate, we denote as type I to type V. Figure 2 shows sketches of these five different types of flow pattern; regions of "downwards" flow (i.e. regions with $u > 0$) are shaded, and regions of "upwards" flow (i.e. regions with $u < 0$) are unshaded. The locations of the maximum and minimum velocities are marked with dots.

When $\tau \geq 0$ the prescribed shear stress acts down the substrate in cooperation with the effect of gravity. As a result, the velocity is downwards throughout the rivulet; we refer to this flow pattern as type I (see Figure 2(a)). The maximum velocity $u = u_{\mathrm{s}}(0) = u_1$ (> 0), where

$$u_1 = h_{\mathrm{m}}\left(\frac{h_{\mathrm{m}}\sin\alpha}{2} + \tau\right), \tag{3.1}$$

occurs on the free surface at $y = 0$, $z = h_{\mathrm{m}}$ and the minimum velocity $u = 0$ occurs on the substrate $z = 0$.

When $\tau < 0$, the prescribed shear stress acts up the substrate in opposition to the effect of gravity, and the competition between these opposing effects leads to more interesting behaviour than in the case $\tau \geq 0$. In particular, we find that, although the velocity can be downwards within the rivulet, it is always upwards near the edges of the rivulet. The non-trivial curve on which $u = 0$, denoted by $z = H(y)$, is given by

$$H = 2\left(h + \frac{\tau}{\sin\alpha}\right). \tag{3.2}$$

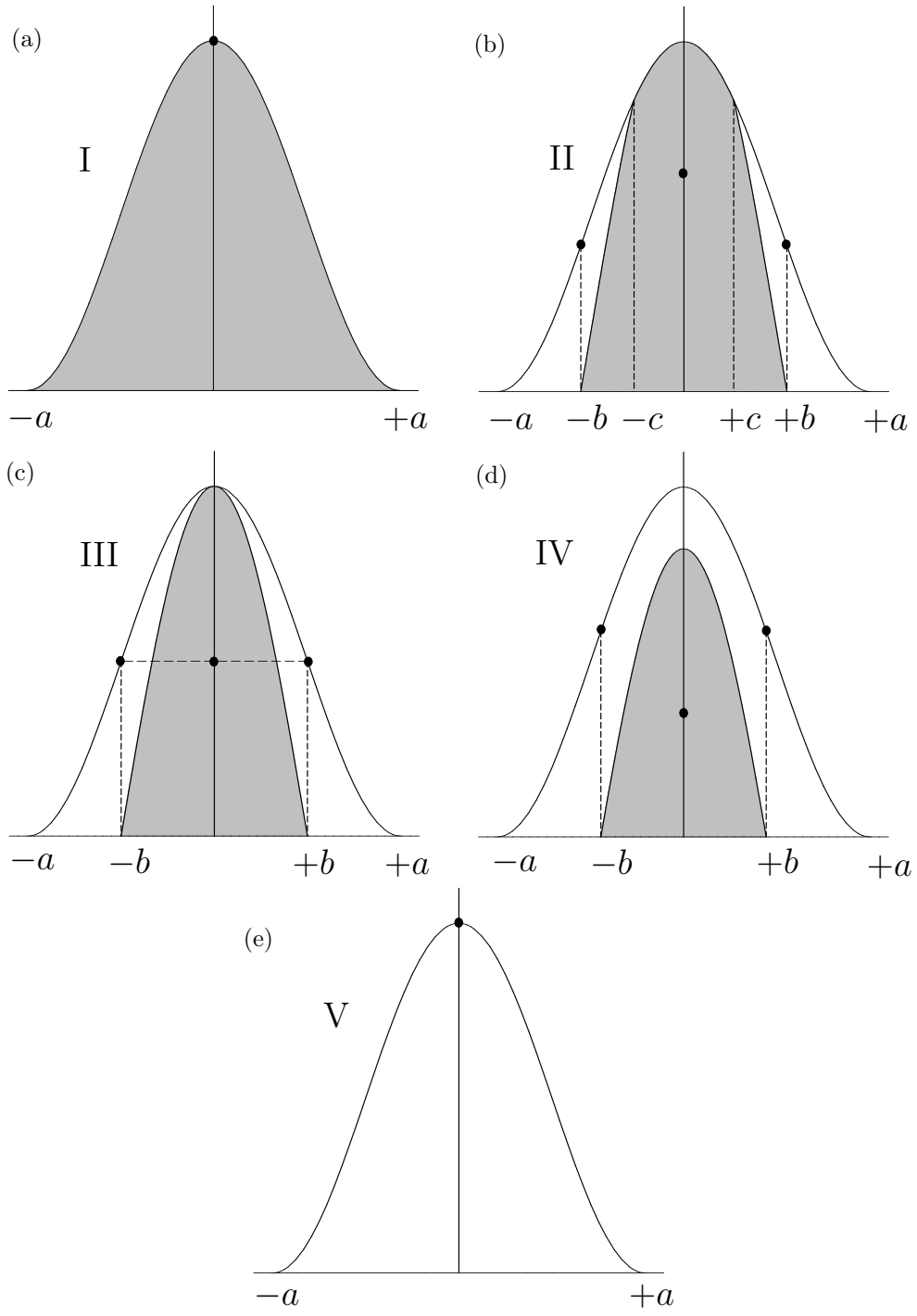

Fig. 2 Sketches of the five different types of cross-sectional flow pattern, denoted as type I to type V. Regions of downwards flow (i.e. regions with $u > 0$) are shaded and regions of upwards flow (i.e. regions with $u < 0$) are unshaded. The locations of the maximum and minimum velocities are marked with dots.

For $h_{\rm m} > h_{\rm V}$, where

$$h_{\rm V} = -\frac{\tau}{\sin\alpha}, \tag{3.3}$$

this curve intersects the y-axis (i.e. $H = 0$) at $y = \pm b$, where

$$b = \frac{1}{m}\cos^{-1}\left(-\frac{2\tau}{h_{\rm m}\sin\alpha} - 1\right) \ (> 0), \tag{3.4}$$

and for $h_{\rm m} > h_{\rm III}$, where

$$h_{\rm III} = -\frac{2\tau}{\sin\alpha}, \tag{3.5}$$

it intersects the free surface (i.e. $H = h$) at $y = \pm c$, where

$$c = \frac{1}{m}\cos^{-1}\left(-\frac{4\tau}{h_{\rm m}\sin\alpha} - 1\right) \ (> 0). \tag{3.6}$$

When $h_{\rm m} > h_{\rm III}$ we have $H_{\rm m} = H(0) > h_{\rm m}$, and we refer to this flow pattern as type II (Figure 2(b)). When $h_{\rm m} = h_{\rm III}$ we have $H_{\rm m} = h_{\rm m}$, $b = a/2$ and $c = 0$, and the curve $z = H$ just touches the free surface at $y = 0$, $z = h_{\rm m}$; we refer to this flow pattern as type III (Figure 2(c)) and note that it is the marginal case between type II and type IV. When $h_{\rm V} < h_{\rm m} < h_{\rm III}$ we have $0 < H_{\rm m} < h_{\rm m}$ and we refer to this flow pattern as type IV (Figure 2(d)). For flow patterns II, III and IV the maximum velocity $u = u(0, H_{\rm m}/2) = u_1 + u_2$ (> 0), where

$$u_2 = \frac{\tau^2}{2\sin\alpha}, \tag{3.7}$$

occurs within the flow at $y = 0$, $z = H_{\rm m}/2 = h_{\rm m} + \tau/\sin\alpha$, and the minimum velocity $u = u_{\rm s}(b) = -u_2$ (< 0) occurs on the free surface at $y = \pm b$, $z = -\tau/\sin\alpha$.

Finally, when $h_{\rm m} \le h_{\rm V}$ the prescribed shear stress dominates the effect of gravity and the velocity is upwards throughout the rivulet; we refer to this flow pattern as type V (Figure 2(e)). The maximum velocity $u = 0$ occurs on the substrate $z = 0$, and the minimum velocity $u = u_{\rm s}(0) = u_1$ (< 0) occurs on the free surface at $y = 0$, $z = h_{\rm m}$.

Four of the five flow patterns are illustrated in Figure 3, which shows the free surface profile and velocity contours in the case $\alpha = 3\pi/4$ and $\bar{Q} = 1$ for $\tau = 0.5$ (type I), $\tau = -0.5$ (type II), $\tau = \tau_{\rm III} \simeq -0.9295$ (type III) and $\tau = -1.5$ (type IV), where

$$\tau_{\rm III} = -\left(\frac{6\bar{Q}m\sin^2\alpha}{\pi}\right)^{\frac{1}{3}} \ (< 0) \tag{3.8}$$

is the critical value of τ corresponding to $h_{\rm m} = h_{\rm III}$. The contour interval is constant and the locations of the maximum and minimum velocities are marked with dots.

4. Rivulet Solutions

Figure 4 shows a sketch of Q given by (2.17) as a function of $h_{\rm m}$ for $\tau > 0$, $\tau = 0$ and $\tau < 0$, and summarises when the different types of flow pattern described in Section 3 occur. For $\tau \ge 0$, Q is a monotonically increasing function of $h_{\rm m}$, tending to infinity as $h_{\rm m} \to \infty$. In

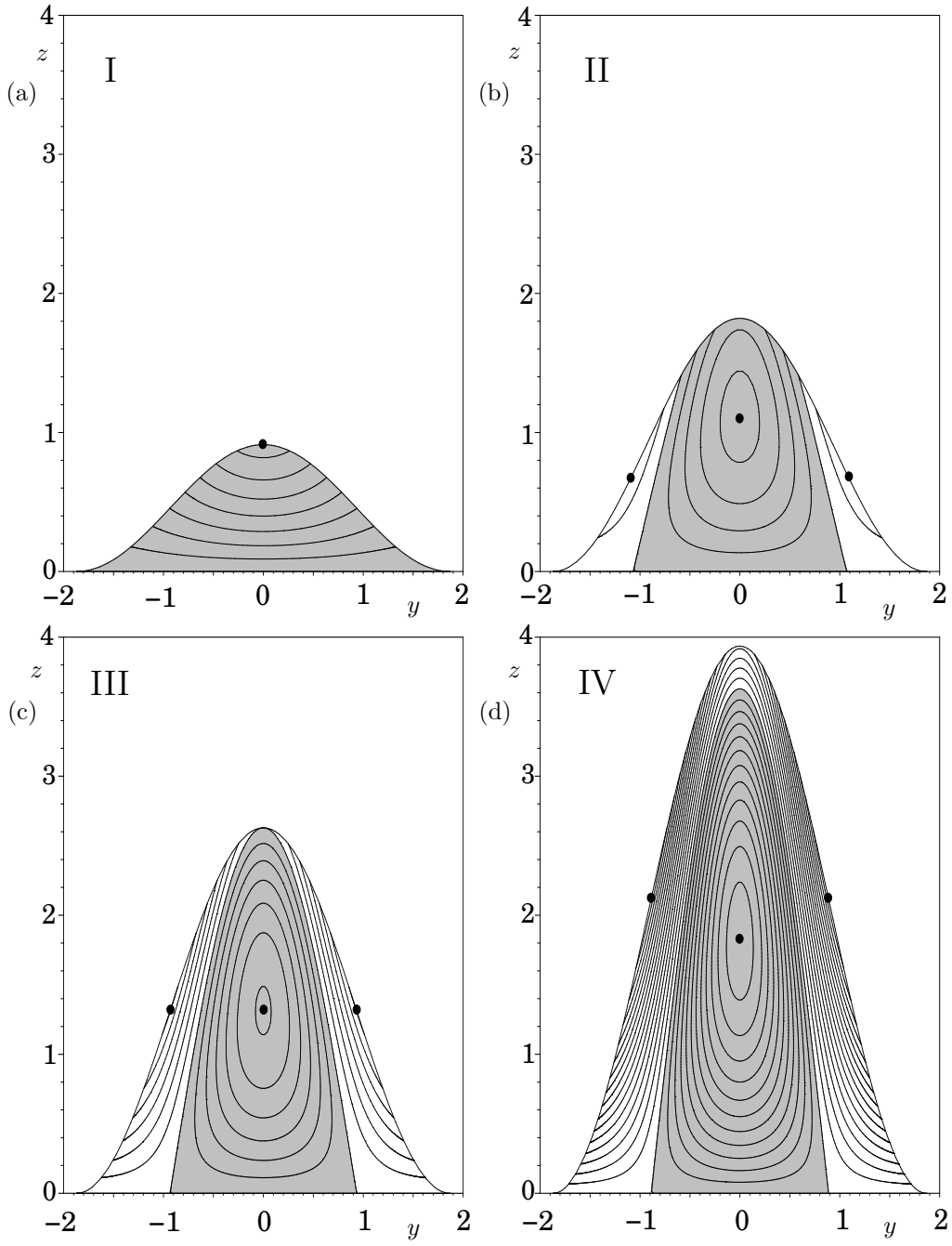

Fig. 3 Free surface profile and velocity contours in the case $\alpha = 3\pi/4$ and $\bar{Q} = 1$ for (a) $\tau = 0.5$ (type I), (b) $\tau = -0.5$ (type II), (c) $\tau = \tau_{\mathrm{III}} \simeq -0.9295$ (type III), and (d) $\tau = -1.5$ (type IV). Regions of downwards flow (i.e. regions with $u > 0$) are shaded and regions of upwards flow (i.e. regions with $u < 0$) are unshaded. The contour interval is constant and the locations of the maximum and minimum velocities are marked with dots.

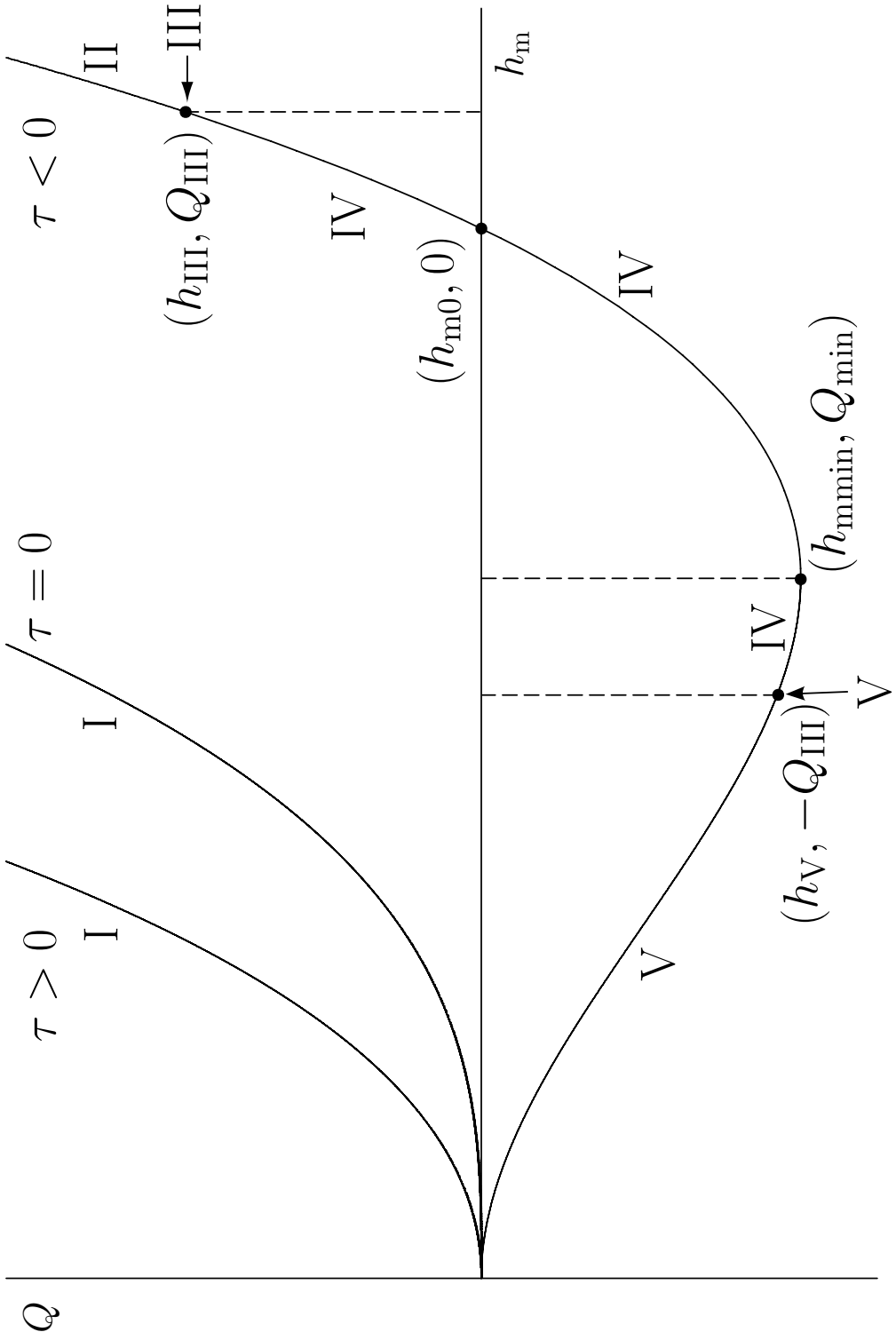

Fig. 4 Sketch of Q as a function of h_{m} for $\tau > 0$, $\tau = 0$ and $\tau < 0$, summarising when the different types of flow pattern occur.

contrast, for $\tau < 0$, Q initially decreases monotonically to a minimum value $Q = Q_{\min}$ at $h_{\mathrm{m}} = h_{\mathrm{mmin}}$, where

$$Q_{\min} = -\frac{9\pi(-\tau)^3}{50m\sin^2\alpha}\ (<0), \quad h_{\mathrm{mmin}} = -\frac{6\tau}{5\sin\alpha}, \tag{4.1}$$

before increasing monotonically through the value $Q = 0$ at $h_{\mathrm{m}} = h_{\mathrm{m0}}$ given by (2.20), and tending to infinity as $h_{\mathrm{m}} \to \infty$.

As Figure 4 shows, the number and nature of solutions for h_{m} depends on the values of τ, α and $\bar{Q}$. When $\tau \geq 0$, there is one solution (of type I) when $\bar{Q} > 0$, but no solutions when $\bar{Q} \leq 0$. When $\tau < 0$, there is one solution when $\bar{Q} \geq 0$ (which is of type II and satisfies $h_{\mathrm{m}} > h_{\mathrm{III}}$ for $\bar{Q} > Q_{\mathrm{III}}$, of type III given by $h_{\mathrm{m}} = h_{\mathrm{III}}$ for $\bar{Q} = Q_{\mathrm{III}}$, and of type IV and satisfies $h_{\mathrm{m0}} \leq h_{\mathrm{m}} < h_{\mathrm{III}}$ for $0 \leq \bar{Q} < Q_{\mathrm{III}}$, where

$$Q_{\mathrm{III}} = \frac{\pi(-\tau)^3}{6m\sin^2\alpha}\ (>0) \tag{4.2}$$

is the critical value of $\bar{Q}$ corresponding to $h_{\mathrm{m}} = h_{\mathrm{III}}$). When $\bar{Q} < 0$ there are two solutions when $Q_{\min} < \bar{Q} < 0$, a "thick" solution (which is of type IV satisfying $h_{\mathrm{mmin}} < h_{\mathrm{m}} < h_{\mathrm{m0}}$) and a "thin" solution (which is of type V satisfying $0 < h_{\mathrm{m}} \leq h_{\mathrm{V}}$ for $-Q_{\mathrm{III}} \leq \bar{Q} < 0$ and of type IV satisfying $h_{\mathrm{V}} < h_{\mathrm{m}} < h_{\mathrm{mmin}}$ for $Q_{\min} < \bar{Q} < -Q_{\mathrm{III}}$), one solution (of type IV given by $h_{\mathrm{m}} = h_{\mathrm{mmin}}$) when $\bar{Q} = Q_{\min}$, and no solutions when $\bar{Q} < Q_{\min}$.

Figure 5 shows how the $\tau/\bar{Q}^{\frac{1}{3}}$–$\alpha$ parameter plane for $\bar{Q} > 0$ is divided into regions in which the solutions have different flow patterns by the α axis and the curve $h_{\mathrm{m}} = h_{\mathrm{III}}$ for $\tau < 0$, and Figure 6 shows how the $\tau/(-\bar{Q})^{\frac{1}{3}}$–$\alpha$ parameter plane for $\bar{Q} < 0$ is divided into regions in which the solutions have different flow patterns by the curve $h_{\mathrm{m}} = h_{\mathrm{V}}$ for $\tau < 0$, and into regions in which there are no or two solutions by the curve $h_{\mathrm{m}} = h_{\mathrm{mmin}}$ for $\tau < 0$ on which there is one solution.

4.1 *Rivulet Solutions for Varying α*

As well as being of interest in their own right, rivulet solutions for varying α can be interpreted as describing flow down a slowly varying substrate such as, for example, flow in the azimuthal direction round the lower part of a large horizontal cylinder.

Whatever the values of τ and $\bar{Q}$, the rivulet semiwidth is given by $a = \pi/m$ and so all rivulets become wide according to

$$a \sim \pi\left(\alpha - \frac{\pi}{2}\right)^{-\frac{1}{2}} \to \infty \tag{4.3}$$

as $\alpha \to \pi/2^+$, and approach the finite semiwidth $a = \pi$ according to

$$a = \pi + \frac{\pi}{4}(\pi - \alpha)^2 + O(\pi - \alpha)^4 \tag{4.4}$$

as $\alpha \to \pi^-$.

Figures 7, 8 and 9 show h_{m} as a function of α in the cases $\tau = 1$, $\tau = 0$ and $\tau = -1$, respectively, for various values of $\bar{Q}$; these are typical of h_{m} for all $\tau > 0$, $\tau = 0$ and $\tau < 0$, respectively.

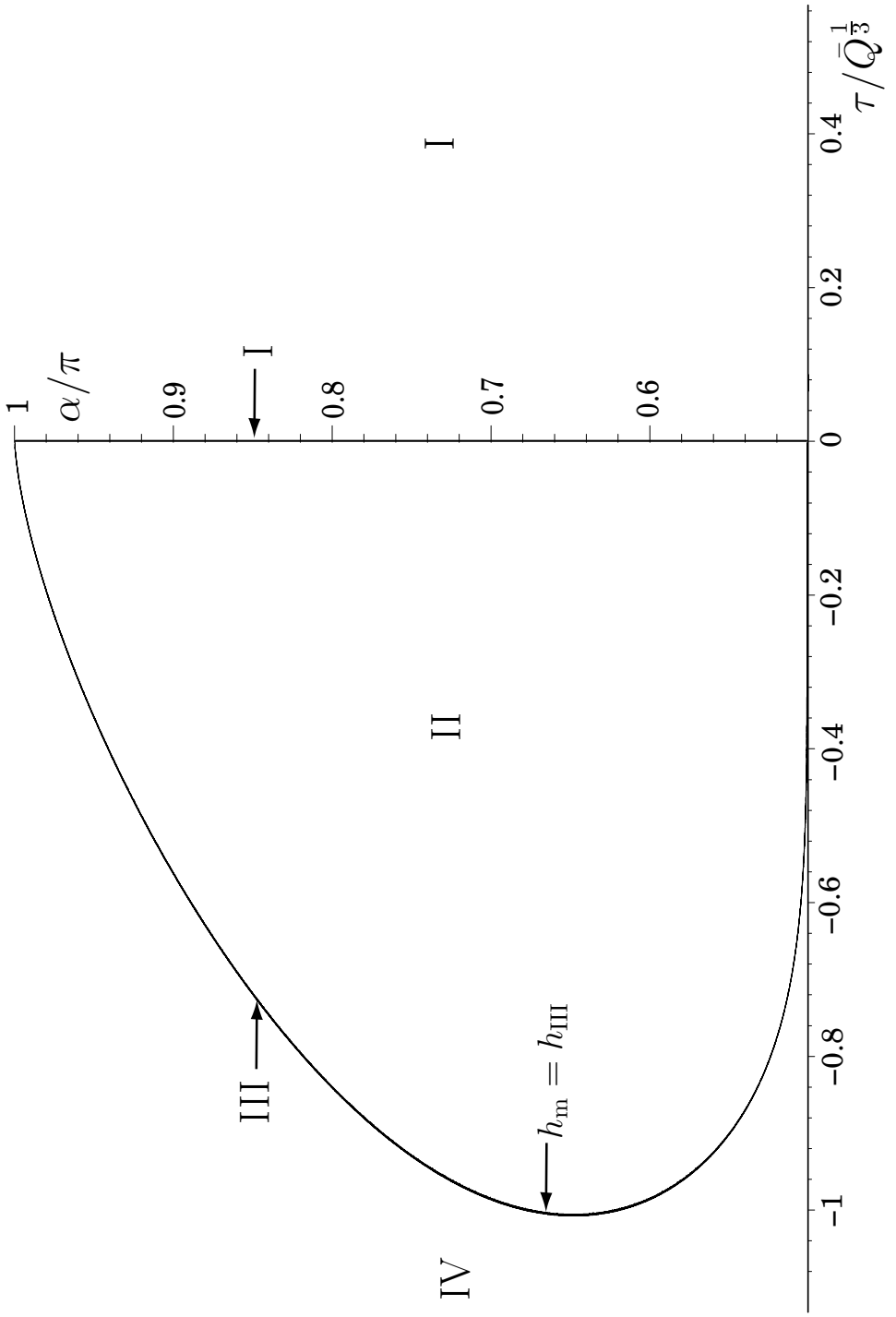

Fig. 5 Plot of the $\tau/\bar{Q}^{\frac{1}{3}}$–$\alpha$ parameter plane for $\bar{Q} > 0$ divided into regions in which the solutions have different flow patterns by the α axis and the curve $h_{\mathrm{m}} = h_{\mathrm{III}}$ for $\tau < 0$.

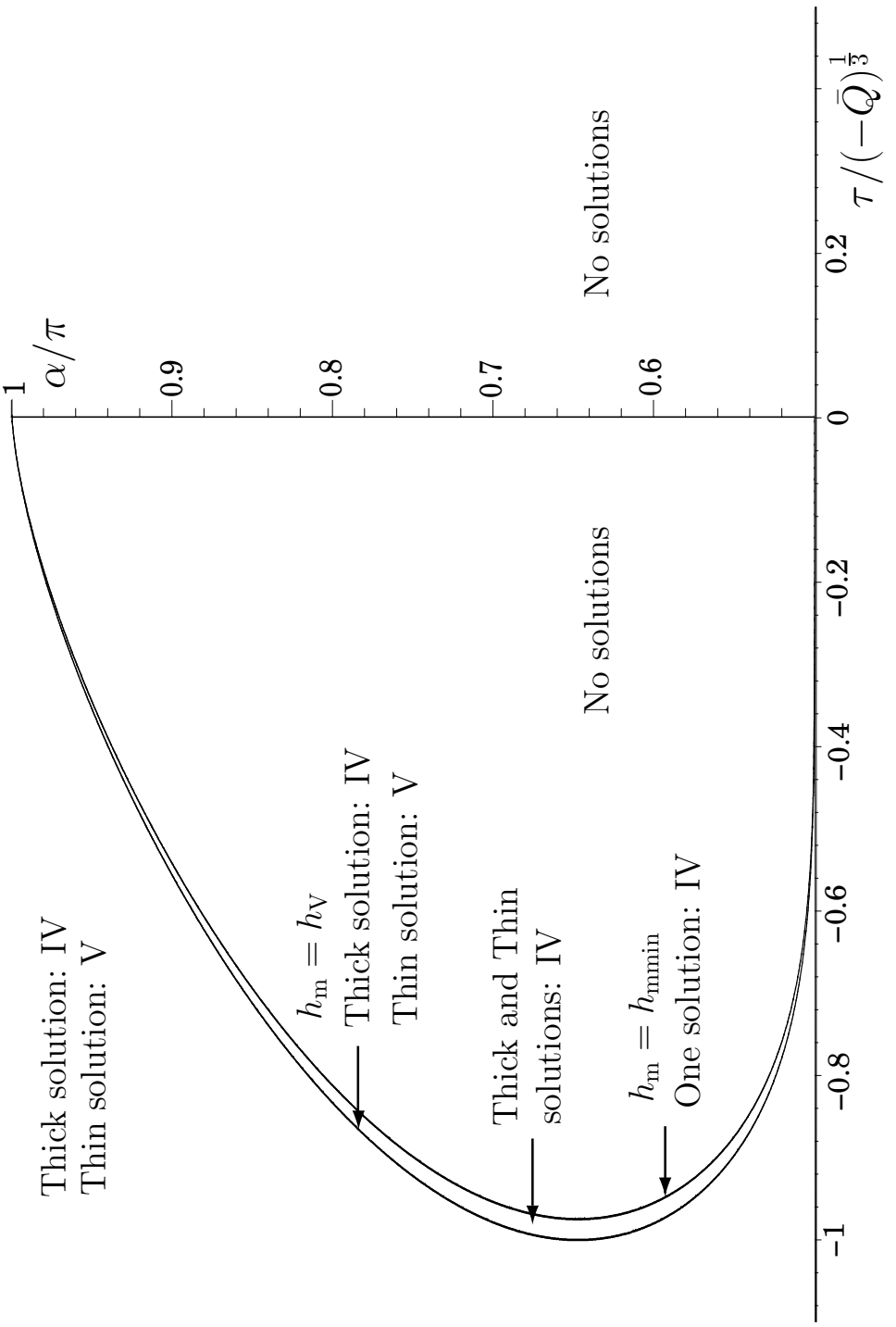

Fig. 6 Plot of the $\tau/(-\bar{Q})^{\frac{1}{3}}$–$\alpha$ parameter plane for $\bar{Q} < 0$ divided into regions in which the solutions have different flow patterns by the curve $h_{\rm m} = h_{\rm V}$ for $\tau < 0$, and into regions in which there are no or two solutions by the curve $h_{\rm m} = h_{\rm mmin}$ for $\tau < 0$ on which there is one solution.

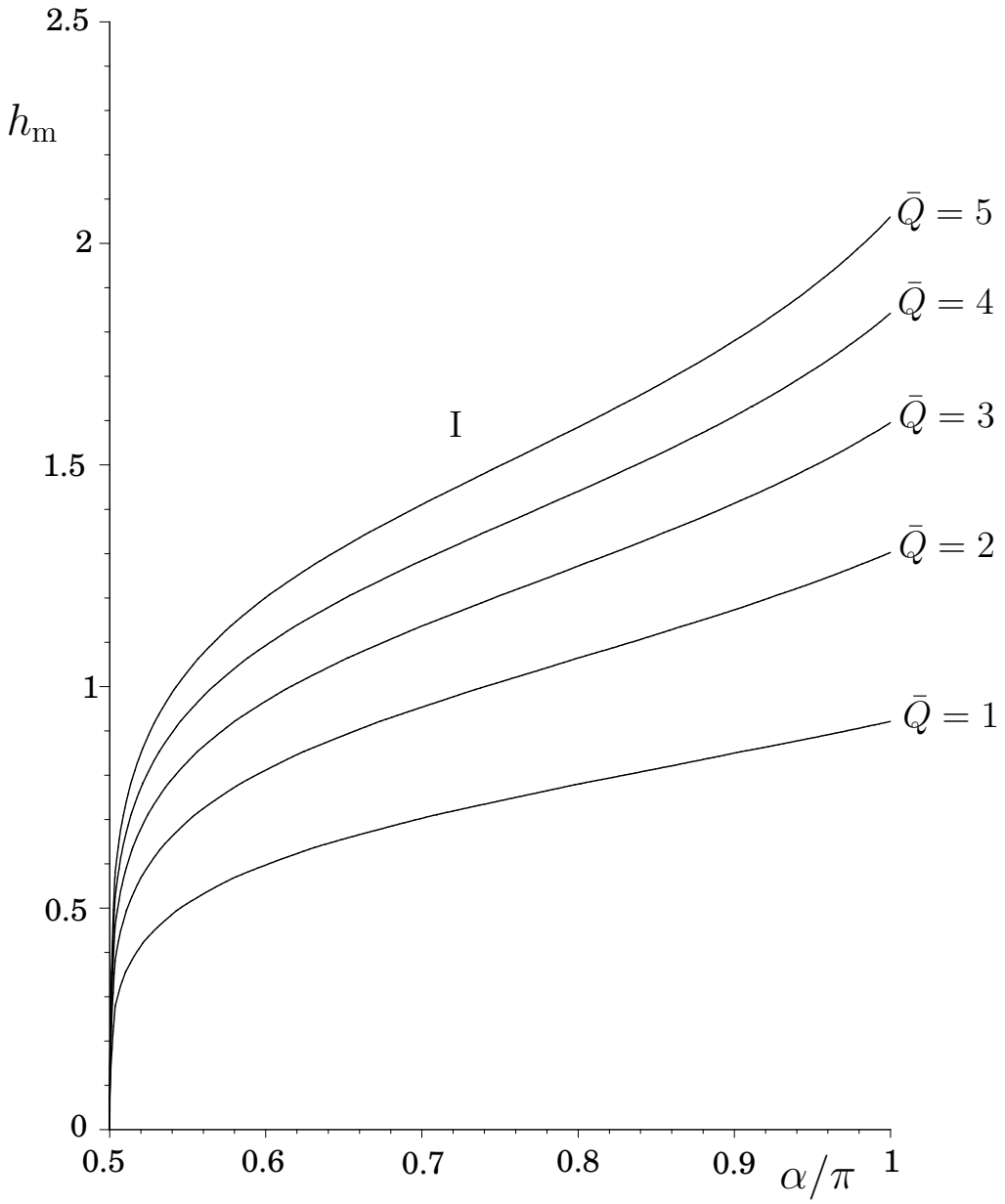

Fig. 7 Plot of h_{m} as a function of α in the case $\tau = 1$ for $\bar{Q} = 1, \ldots, 5$. All solutions are of type I.

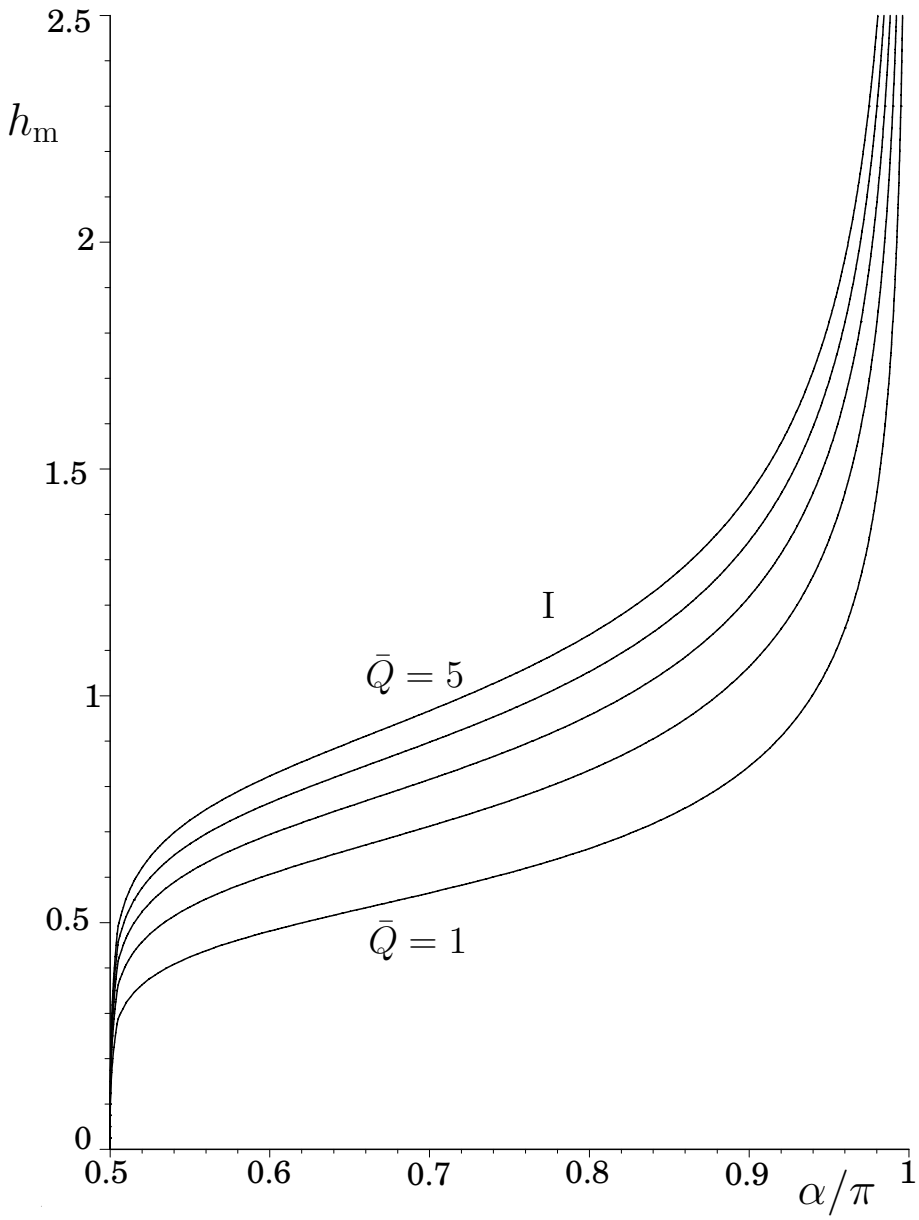

Fig. 8 Plot of h_{m} as a function of α in the special case $\tau = 0$ for $\bar{Q} = 1, \ldots, 5$. All solutions are of type I.

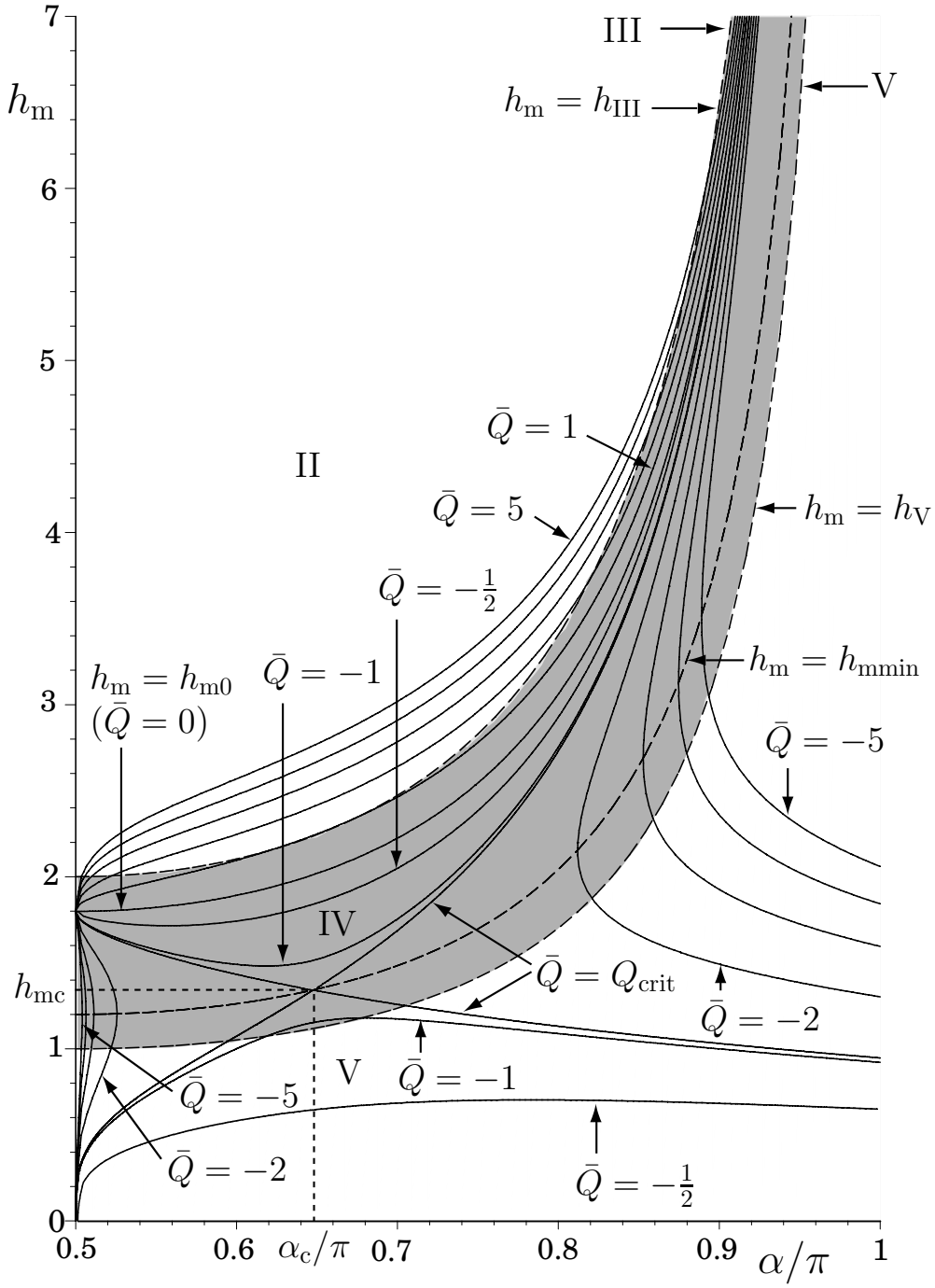

Fig. 9 Plot of $h_{\rm m}$ as a function of α in the case $\tau = -1$ for $\bar{Q} = -5, \ldots, 5$. Also shown are regions in which the solutions have different flow patterns divided by the curves $h_{\rm m} = h_{\rm III}$ and $h_{\rm m} = h_{\rm V}$ (shown with dashed curves), and the curve $h_{\rm m} = h_{\rm mmin}$ (also shown with a dashed curve). For clarity, the region in which the solutions are of type IV is shaded.

4.1.1 $\tau > 0$

Figure 7 shows h_m as a function of α in the case $\tau = 1$ for $\bar{Q} = 1, \ldots, 5$. There is a single solution for h_m everywhere (i.e. for all $\pi/2 < \alpha \leq \pi$) for each value of $\bar{Q}$ (> 0) and all solutions are of type I. In this case (i.e. when $\tau > 0$) the rivulets become shallow according to

$$h_\mathrm{m} \sim \left(\frac{8\bar{Q}}{3\pi\tau}\right)^{\frac{1}{2}} \left(\alpha - \frac{\pi}{2}\right)^{\frac{1}{4}} \to 0^+ \tag{4.5}$$

as $\alpha \to \pi/2^+$, and approach the finite height $h_\mathrm{m} = h_{\mathrm{m}\pi} = (8\bar{Q}/3\pi\tau)^{\frac{1}{2}}$ according to

$$h_\mathrm{m} = h_{\mathrm{m}\pi} - \frac{20\bar{Q}}{27\pi\tau^2}(\pi - \alpha) + O(\pi - \alpha)^2 \tag{4.6}$$

as $\alpha \to \pi^-$.

4.1.2 $\tau = 0$

Figure 8 shows h_m given by (2.18) as a function of α in the special case $\tau = 0$ for $\bar{Q} = 1, \ldots, 5$. There is again a single solution for h_m everywhere (i.e. for all $\pi/2 < \alpha \leq \pi$) for each value of $\bar{Q}$ (> 0) and all solutions are of type I. In this case (i.e. when $\tau = 0$) the rivulets become shallow according to

$$h_\mathrm{m} \sim \left(\frac{24\bar{Q}}{5\pi}\right)^{\frac{1}{3}} \left(\alpha - \frac{\pi}{2}\right)^{\frac{1}{6}} \to 0^+ \tag{4.7}$$

as $\alpha \to \pi/2^+$, and become deep (and hence the assumption that the rivulet is sufficiently slowly varying in α ultimately fails) according to

$$h_\mathrm{m} \sim \left(\frac{24\bar{Q}}{5\pi}\right)^{\frac{1}{3}} (\pi - \alpha)^{-\frac{1}{3}} \to \infty \tag{4.8}$$

as $\alpha \to \pi^-$.

4.1.3 $\tau < 0$

Figure 9 shows h_m as a function of α in the case $\tau = -1$ for $\bar{Q} = -5, \ldots, 5$, and, as expected, reveals that the behaviour when $\tau < 0$ is more complicated than when $\tau \geq 0$. Specifically, for each value of $\bar{Q} \geq 0$, there is a single solution for h_m everywhere (i.e. for all $\pi/2 < \alpha \leq \pi$) satisfying $h_\mathrm{m} \geq h_{\mathrm{m}0}$. However, when $\bar{Q} < 0$ there can be one, two or no solutions for h_m (all satisfying $h_\mathrm{m} < h_{\mathrm{m}0}$) depending on the values of τ, α and $\bar{Q}$. For $Q_\mathrm{crit} < \bar{Q} < 0$, where

$$Q_\mathrm{crit} = -\frac{9 \times 5^{\frac{1}{4}}\pi(-\tau)^3}{40} \simeq -1.0570(-\tau)^3 \ (< 0), \tag{4.9}$$

there are two disconnected branches of solutions for h_m, each of which extends all the way from $\alpha = \pi/2^+$ to $\alpha = \pi$, that is, there is both a thick and a thin solution everywhere. As $\bar{Q}$ decreases from zero towards Q_crit these two branches of solutions move closer together, and when $\bar{Q} = Q_\mathrm{crit}$ they meet at $\alpha = \alpha_\mathrm{c} = \pi - \tan^{-1} 2 \simeq 0.6476\pi$, with $h_\mathrm{m} = h_\mathrm{mc} =$

$h_{\mathrm{mmin}}(\alpha_{\mathrm{c}}) = -3\tau/\sqrt{5} \simeq -1.3416\tau$ (> 0). For $\bar{Q} < Q_{\mathrm{crit}}$ there are again two disconnected branches of solutions for h_{m}, but now with each branch comprising a thick and a thin solution, which coincide at $\alpha = \alpha_1$ and $\alpha = \alpha_2$ with $h_{\mathrm{m}} = h_{\mathrm{mmin}}(\alpha_1)$ and $h_{\mathrm{m}} = h_{\mathrm{mmin}}(\alpha_2)$, respectively, where α_1 and α_2 $(> \alpha_1)$ are the appropriate solutions of $\bar{Q} = Q_{\mathrm{min}}$; thus there are no solutions for $\alpha_1 < \alpha < \alpha_2$, one solution at $\alpha = \alpha_1$ and $\alpha = \alpha_2$, and two solutions for $\pi/2 < \alpha < \alpha_1$ and $\alpha_2 < \alpha \leq \pi$. Thus, unlike the case $\tau \geq 0$ in which a slowly varying rivulet can run continuously round the lower part of a large horizontal cylinder from $\alpha = \pi/2^+$ to $\alpha = \pi$ for *any* $\bar{Q}$ (> 0), when $\tau < 0$ this can happen only when $\bar{Q} \geq Q_{\mathrm{crit}}$.

In this case (i.e. when $\tau < 0$) both the single solution for $\bar{Q} \geq 0$ and the thick solution for $\bar{Q} < 0$ approach the finite height $h_{\mathrm{m}} = h_{\mathrm{m}\frac{\pi}{2}} = -9\tau/5$ according to

$$h_{\mathrm{m}} = h_{\mathrm{m}\frac{\pi}{2}} + \frac{40\bar{Q}}{27\pi\tau^2}\left(\alpha - \frac{\pi}{2}\right)^{\frac{1}{2}} + O\left(\alpha - \frac{\pi}{2}\right) \tag{4.10}$$

as $\alpha \to \pi/2^+$, while the thin solution for $\bar{Q} < 0$ becomes shallow according to (4.5) as $\alpha \to \pi/2^+$. Similarly, both the single solution for $\bar{Q} \geq 0$ and the thick solution for $\bar{Q} < 0$ become deep according to

$$h_{\mathrm{m}} \sim -\frac{9\tau}{5\,(\pi - \alpha)} \to \infty \tag{4.11}$$

as $\alpha \to \pi^-$, while the thin solution for $\bar{Q} < 0$ approaches the finite height $h_{\mathrm{m}} = h_{\mathrm{m}\pi} = (8\bar{Q}/3\pi\tau)^{\frac{1}{2}}$ according to (4.6) as $\alpha \to \pi^-$.

In the special case $\bar{Q} = Q_{\mathrm{crit}}$ the fact that the two branches of solutions meet at $\alpha = \alpha_{\mathrm{c}}$ means that four different kinds of behaviour are possible for varying α: a rivulet could be thin everywhere, thick everywhere, thin in $\pi/2 < \alpha < \alpha_{\mathrm{c}}$ and thick in $\alpha_{\mathrm{c}} < \alpha \leq \pi$, or thick in $\pi/2 < \alpha < \alpha_{\mathrm{c}}$ and thin in $\alpha_{\mathrm{c}} < \alpha \leq \pi$. In the first two cases the rivulet has a corner at $\alpha = \alpha_{\mathrm{c}}$[†], whereas in the latter two cases the rivulet is smooth at $\alpha = \alpha_{\mathrm{c}}$.

Figure 9 also shows how the α–h_{m} parameter plane is divided into regions in which the solutions have different flow patterns by the critical curves $h_{\mathrm{m}} = h_{\mathrm{III}}$ and $h_{\mathrm{m}} = h_{\mathrm{V}}$ (shown with dashed curves). In particular, when $\bar{Q} > Q_{\mathrm{IIIc}}$, where

$$Q_{\mathrm{IIIc}} = \frac{5^{\frac{5}{4}}\pi(-\tau)^3}{24} \simeq 0.9787(-\tau)^3 \ (> 0) \tag{4.12}$$

is the value of Q_{III} given by (4.2) at $\alpha = \alpha_{\mathrm{c}}$, solutions are of type II for $\alpha_{\mathrm{III1}} < \alpha < \alpha_{\mathrm{III2}}$, type III at $\alpha = \alpha_{\mathrm{III1}}$ and $\alpha = \alpha_{\mathrm{III2}}$, and type IV elsewhere, where α_{III1} and α_{III2} $(> \alpha_{\mathrm{III1}})$ are the appropriate solutions of $\bar{Q} = Q_{\mathrm{III}}$ and satisfy $\alpha_{\mathrm{III1}} < \alpha_{\mathrm{c}} < \alpha_{\mathrm{III2}}$. When $\bar{Q} = Q_{\mathrm{IIIc}}$ solutions are of type IV everywhere except at $\alpha = \alpha_{\mathrm{c}}$ (where they are of type III), and when $0 \leq \bar{Q} < Q_{\mathrm{IIIc}}$ they are of type IV everywhere. When $\bar{Q} < 0$ all thick solutions are of type IV everywhere, while thin solutions for $-Q_{\mathrm{IIIc}} \leq \bar{Q} < 0$ are of type V everywhere and thin solutions for $\bar{Q} < -Q_{\mathrm{IIIc}}$ are of type IV for $\alpha_{\mathrm{III1}} < \alpha < \alpha_{\mathrm{III2}}$ and of type V elsewhere.

Thus the flow pattern within a slowly varying rivulet may change as it flows round the lower part of a large horizontal cylinder. For a rivulet with $\bar{Q} > Q_{\mathrm{IIIc}}$ the flow pattern changes from type IV for $\pi/2 < \alpha < \alpha_{\mathrm{III1}}$ to type III at $\alpha = \alpha_{\mathrm{III1}}$, to type II for $\alpha_{\mathrm{III1}} <$

[†] This corner in the critical rivulet is analogous to the well known corner in the critical solution in coating and rimming flow of a thin film of fluid on a uniformly rotating horizontal cylinder found by Moffatt (**28**) and analysed by Wilson, Hunt and Duffy (**29**).

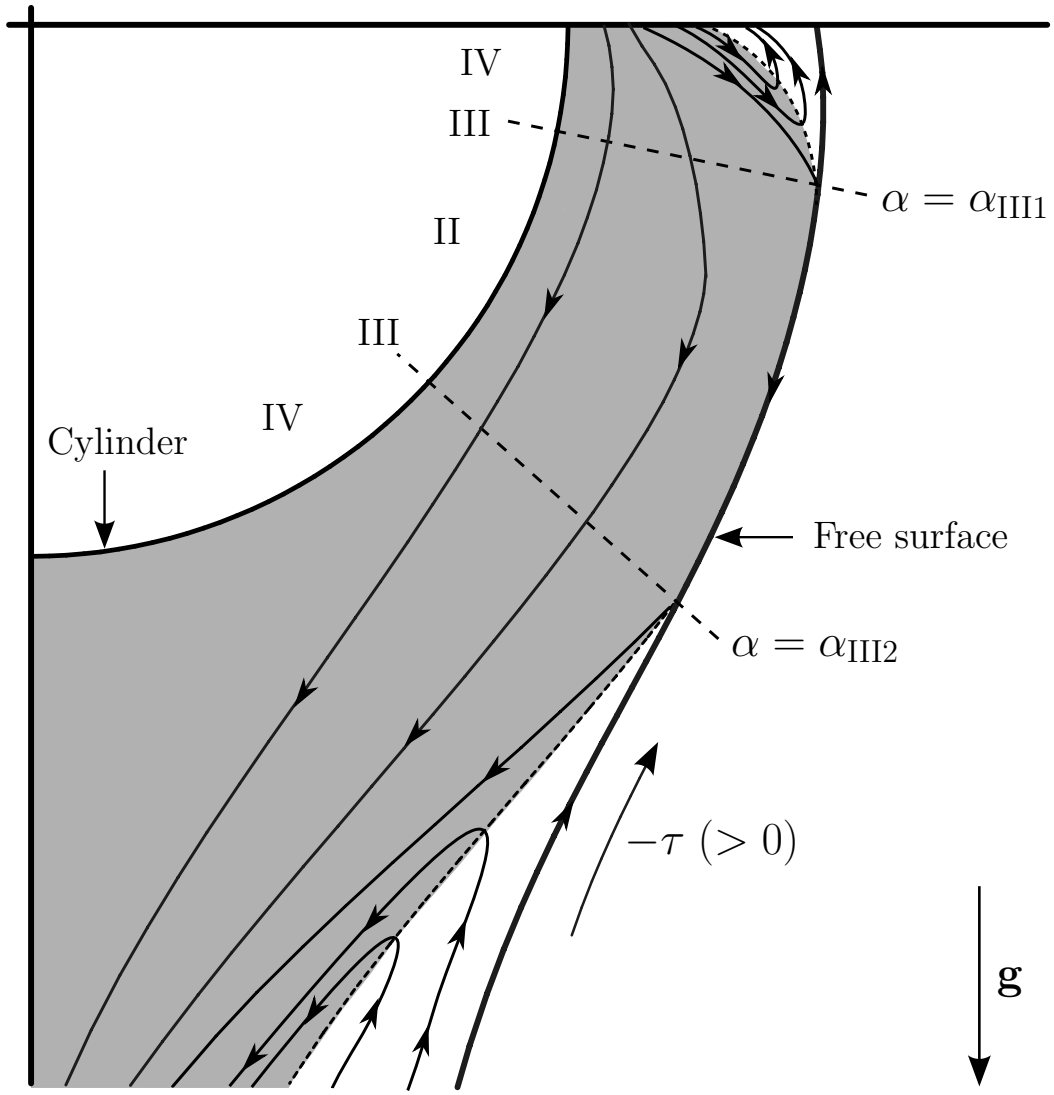

Fig. 10 Sketch of the streamline pattern in the symmetry plane, $y = 0$, of a slowly varying rivulet on the lower part of a large horizontal cylinder when $\tau < 0$ in the case $\bar{Q} > Q_{\mathrm{IIIc}}$. Regions of downwards flow (i.e. regions with $u > 0$) are shaded and regions of upwards flow (i.e. regions with $u < 0$) are unshaded.

$\alpha < \alpha_{\mathrm{III}2}$, to type III at $\alpha = \alpha_{\mathrm{III}2}$, to type IV for $\alpha_{\mathrm{III}2} < \alpha \leq \pi$. On the other hand, for a thin rivulet with $Q_{\mathrm{crit}} \leq \bar{Q} < -Q_{\mathrm{IIIc}}$ the flow pattern changes from type V for $\pi/2 < \alpha \leq \alpha_{\mathrm{III}1}$ to type IV for $\alpha_{\mathrm{III}1} < \alpha < \alpha_{\mathrm{III}2}$, to type V for $\alpha_{\mathrm{III}2} \leq \alpha \leq \pi$, where $\alpha_{\mathrm{III}1}$ and $\alpha_{\mathrm{III}2}$ satisfy $\alpha_{\mathrm{IIImin}} \leq \alpha_{\mathrm{III}1} < \alpha_{\mathrm{c}}$ and $\alpha_{\mathrm{c}} < \alpha_{\mathrm{III}2} \leq \alpha_{\mathrm{IIImax}}$, where $\alpha_{\mathrm{IIImin}} \simeq 0.5950\pi$ and $\alpha_{\mathrm{IIImax}} \simeq 0.7051\pi$ are the appropriate solutions of the simultaneous equations $h_{\mathrm{m}} = h_{\mathrm{V}}$

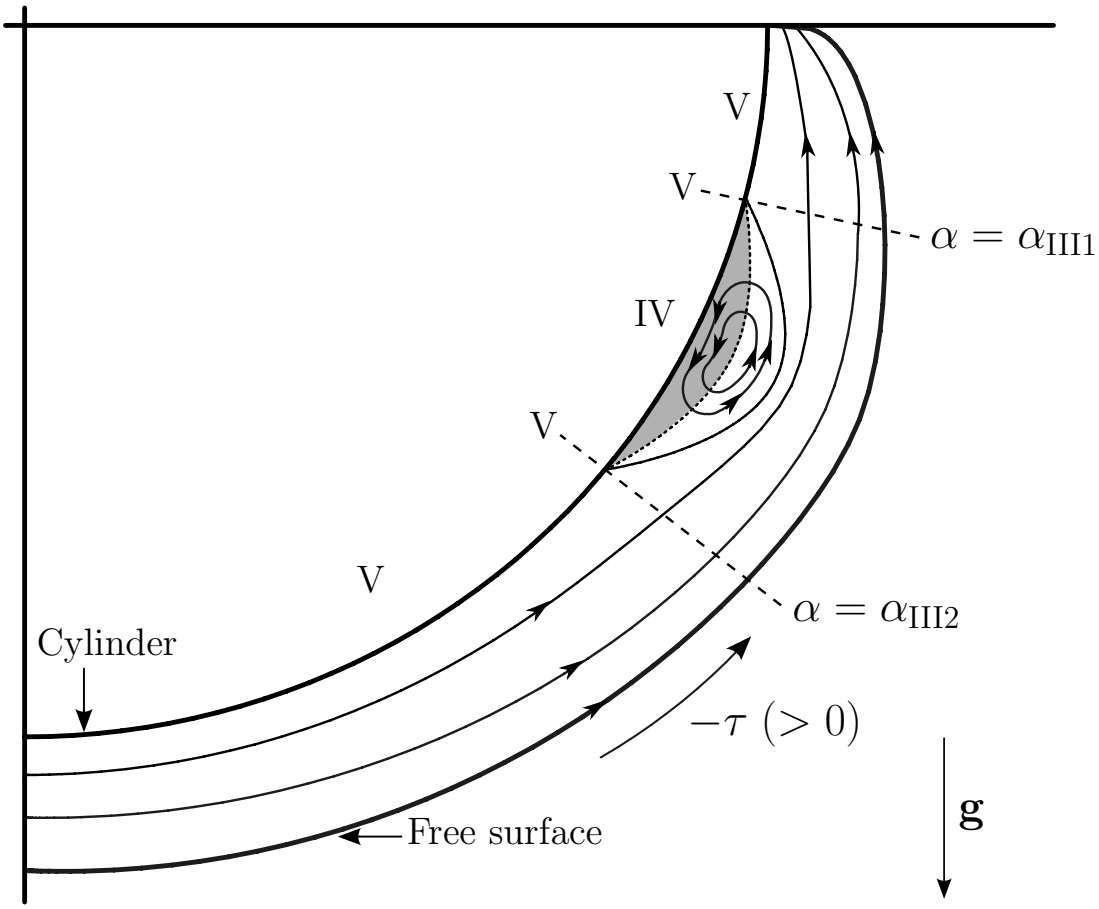

Fig. 11 Sketch of the streamline pattern in the symmetry plane, $y = 0$, of a slowly varying rivulet on the lower part of a large horizontal cylinder when $\tau < 0$ in the case $Q_{\mathrm{crit}} < \bar{Q} < -Q_{\mathrm{IIIc}}$. Regions of downwards flow (i.e. regions with $u > 0$) are shaded and regions of upwards flow (i.e. regions with $u < 0$) are unshaded.

and $\bar{Q} = Q_{\mathrm{crit}}$. The streamline patterns in the symmetry plane of the rivulet, $y = 0$, are sketched Figures 10 and 11, respectively, in these two cases. In particular, Figure 10 shows the regions of backflow that will occur in $\pi/2 < \alpha < \alpha_{\mathrm{III}1}$ and $\alpha_{\mathrm{III}2} < \alpha \leq \pi$ for $\bar{Q} > Q_{\mathrm{IIIc}}$, and Figure 11 shows the recirculation "bubble" of "trapped" fluid in $\alpha_{\mathrm{III}1} < \alpha < \alpha_{\mathrm{III}2}$ that will occur for $Q_{\mathrm{crit}} \leq \bar{Q} < -Q_{\mathrm{IIIc}}$, as consequences of the competition between the (downwards) effect of gravity and the (upwards) effect of the prescribed shear stress. The "footprints" on the substrate of the regions of backflow in Figure 10 and of the recirculation region in Figure 11 are given by $|y| \leq b$, where b $(\leq a)$ is defined by (2.17) and (3.4) with $Q = \bar{Q}$; in particular, these regions do not occupy the full width of the rivulet.

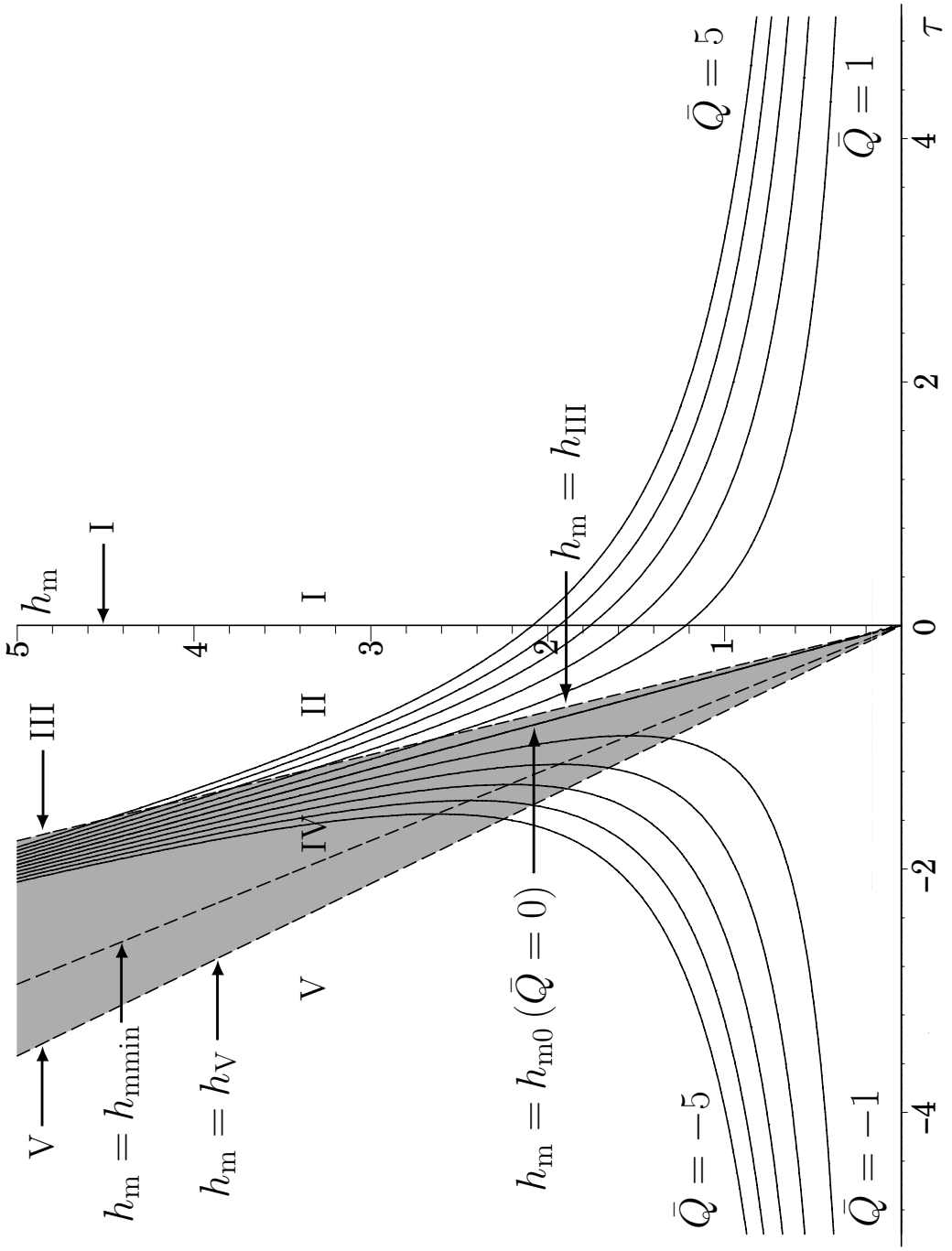

Fig. 12 Plot of $h_{\rm m}$ as a function of τ in the case $\alpha = 3\pi/4$ for $\bar{Q} = -5, \ldots, 5$. Also shown are regions in which the solutions have different flow patterns divided by the curves $h_{\rm m} = h_{\rm III}$ and $h_{\rm m} = h_{\rm V}$ (shown with dashed curves), and the curve $h_{\rm m} = h_{\rm mmin}$ (also shown with a dashed curve). For clarity, the region in which the solutions are of type IV is shaded.

4.2 *Rivulet Solutions for Varying τ*

Rivulet solutions for varying τ can be interpreted as describing flow in the presence of an external airflow exerting a uniform shear stress whose strength varies slowly in time.

Figure 12 shows $h_{\rm m}$ as a function of τ in the case $\alpha = 3\pi/4$ for $\bar{Q} = -5, \ldots, 5$ which is typical of $h_{\rm m}$ for all $\pi/2 < \alpha \leq \pi$.

As Figure 12 shows, for $\bar{Q} \geq 0$ there is a single solution for $h_{\rm m}$ for all τ. In the limit of large positive shear stress, $\tau \to \infty$, the rivulet becomes shallow according to

$$h_{\rm m} \sim \left(\frac{8\bar{Q}m}{3\pi\tau}\right)^{\frac{1}{2}} \to 0^{+}, \tag{4.13}$$

while in the limit of large negative shear stress, $\tau \to -\infty$, the rivulet becomes deep according to

$$h_{\rm m} \sim h_{\rm m0} = -\frac{9\tau}{5\sin\alpha} \to \infty. \tag{4.14}$$

In the limit of small shear stress, $\tau \to 0$, the rivulet approaches the finite height in the case $\tau = 0$ given by (2.18) according to

$$h_{\rm m} = \left(\frac{24\bar{Q}m}{5\pi\sin\alpha}\right)^{\frac{1}{3}} - \frac{3\tau}{5\sin\alpha} + O(\tau^2). \tag{4.15}$$

As Figure 12 also shows, for $\bar{Q} < 0$ there are no solutions for $h_{\rm m}$ when $\tau_{\rm min} < \tau \leq 0$, one solution $h_{\rm m} = h_{\rm mmin}$ when $\tau = \tau_{\rm min}$, and two solutions (one thin and one thick) when $\tau < \tau_{\rm min}$, where

$$\tau_{\rm min} = \left(\frac{50\bar{Q}m\sin^2\alpha}{9\pi}\right)^{\frac{1}{3}} \quad (< 0) \tag{4.16}$$

is the critical value of τ corresponding to $\bar{Q} = Q_{\rm min}$. In the limit of large negative shear stress, $\tau \to -\infty$, the thin rivulet becomes shallow according to (4.13) and the thick rivulet becomes deep according to (4.14).

Figure 12 also shows how the τ–$h_{\rm m}$ parameter plane is divided into regions in which the solutions have different flow patterns by the critical curves $h_{\rm m} = h_{\rm III}$ and $h_{\rm m} = h_{\rm V}$ (shown with dashed curves).

5. Quasi-Steady Stability

Having determined and classified all of the possible rivulet solutions, the next step is to consider whether or not these rivulets are stable.

A full stability analysis is beyond the scope of the present work, but we can make useful progress by considering the quasi-steady stability of a rivulet to small symmetric perturbations, i.e. the stability to symmetric perturbations in the limit in which the contact line moves slowly relative to the bulk of the fluid.

A perturbation to a steady rivulet with zero contact angle will, in general, lead to an unsteady rivulet with a non-zero contact angle. Thus we consider the quasi-steady stability of a pendent rivulet with static contact angle θ_0 (> 0) and semi-width a_0 on a substrate inclined at an angle α to the horizontal ($\pi/2 < \alpha \leq \pi$) subject to a prescribed longitudinal surface shear stress τ in the perfectly wetting limit, $\theta_0 \to 0$.

Following the approach of the earlier work on the quasi-steady stability of a rivulet of non-perfectly wetting fluid by Wilson and Duffy (**30**, **19**), we assume that the flow remains symmetric and unidirectional, and that the quasi-steady motion is driven by that of the moving contact line $y = a$, where $a = a(t)$. We assume that the speed of the moving contact line, a', and the dynamic contact angle, $\theta = \theta(t)$, are related by an empirically determined "Tanner Law" in the rather general form $a' = F(\theta)$, where the function $F = F(\theta)$ satisfies $F(\theta_0) = 0$ and is monotonically increasing near $\theta = \theta_0$. We perturb the basic state with semi-width $a = a_0$ and contact angle $\theta = \theta_0$ by writing $a(t) = a_0 + a_1(t)$ and $\theta(t) = \theta_0 + \theta_1(t)$, where $|a_1| \ll a_0$ and $|\theta_1| \ll \theta_0$ are small perturbations, so that

$$a_1' = \frac{M\theta_1^r}{r!}, \tag{5.1}$$

where $M = \mathrm{d}^r F/\mathrm{d}\theta^r \,|_{\theta=\theta_0}$ (> 0) is the first non-zero (odd) derivative of $F(\theta)$ evaluated at $\theta = \theta_0$. The perturbed rivulet must satisfy the prescribed flux condition $Q = \bar{Q}$, where Q is given by the general expression for a rivulet with non-zero contact angle derived in Section 2, namely (2.14), and hence

$$a_1 \frac{\partial Q}{\partial a} + \theta_1 \frac{\partial Q}{\partial \theta} = 0 \tag{5.2}$$

evaluated at $a = a_0$ and $\theta = \theta_0$, meaning that

$$\theta_1 = \sigma a_1, \tag{5.3}$$

where σ is given by

$$\sigma = -\left.\frac{\partial Q/\partial a}{\partial Q/\partial \theta}\right|_{a=a_0,\theta=\theta_0} = -\frac{m\theta_0\left[2\theta_0 \sin\alpha f'(ma_0) + 9m\tau g'(ma_0)\right]}{6\left[\theta_0 \sin\alpha f(ma_0) + 3m\tau g(ma_0)\right]}, \tag{5.4}$$

in which the functions $f(ma)$ and $g(ma)$ are given by (2.15) and (2.16), respectively. Combining (5.1) and (5.3) the equation satisfied by a_1 is

$$a_1' = \frac{M(\sigma a_1)^r}{r!}, \tag{5.5}$$

so that a_1 is given by

$$a_1 = a_1(0) \begin{cases} e^{\sigma M t} & \text{if} \quad r = 1, \\ \left[1 - \dfrac{(r-1)M\sigma^r}{r!(a_1(0))^{1-r}} t\right]^{\frac{1}{1-r}} & \text{if} \quad r = 3, 5, 7, \ldots, \end{cases} \tag{5.6}$$

where $a_1(0)$ is the value of a_1 at $t = 0$. Hence small perturbations grow or decay exponentially when $r = 1$ and algebraically when $r = 3, 5, 7, \ldots$, and (since both M and r are positive), the stability of the rivulet depends only on the sign of σ. In the perfectly wetting limit, $\theta_0 \to 0$, the semi-width of the basic state $a = a_0$ approaches the value π/m in (2.10) according to

$$a_0 = \frac{\pi}{m} + \frac{\theta_0}{\sigma} + O(\theta_0^2), \tag{5.7}$$

and at leading order the flux Q is given by

$$Q = -\frac{5\pi \sin\alpha}{3m^7}\sigma^3 + \frac{3\pi\tau}{2m^5}\sigma^2. \tag{5.8}$$

Then the equation $Q = \bar{Q}$ with Q given by (5.8) yields a cubic polynomial equation for σ, namely

$$10\pi \sin\alpha\, \sigma^3 - 9\pi\tau m^2\sigma^2 + 6\bar{Q}m^7 = 0. \tag{5.9}$$

For the rivulet not to be unstable we require all the real roots of (5.9) to be negative (for stability) or zero (for neutral stability). When $\bar{Q} > 0$ equation (5.9) has three real roots when $\tau \geq \tau_{\rm s}$ (two of them positive and one negative), and has one (negative) real root and two complex roots when $\tau < \tau_{\rm s}$, where

$$\tau_{\rm s} = \left(\frac{50\bar{Q}m\sin^2\alpha}{9\pi}\right)^{\frac{1}{3}} \ (>0); \tag{5.10}$$

hence, in this case the rivulet is stable when $\tau < \tau_{\rm s}$ and unstable when $\tau \geq \tau_{\rm s}$. When $\bar{Q} = 0$ (and hence necessarily $\tau < 0$) equation (5.9) always has three real roots (one of them negative and the other two zero); hence, in this case the rivulet is always neutrally stable. When $\bar{Q} < 0$ (and hence necessarily $\tau < 0$) equation (5.9) always has one positive real root; hence, in this case the rivulet is always unstable.

Figure 13 shows how the τ–$h_{\rm m}$ parameter plane is divided into stable (shaded) and unstable (unshaded) regions according to the present quasi-steady stability analysis. Specifically, Figure 13 shows that for $\tau > 0$ rivulets with $h_{\rm m} \leq h_{\rm ms}$ are unstable and rivulets with $h_{\rm m} > h_{\rm ms}$ are stable, where

$$h_{\rm ms} = \frac{3\tau}{5\sin\alpha} \tag{5.11}$$

is the critical value of $h_{\rm m}$ corresponding to $\tau = \tau_{\rm s}$. Figure 13 also shows that for $\tau \leq 0$ rivulets with $h_{\rm m} > h_{\rm m0}$, $h_{\rm m} = h_{\rm m0}$ and $h_{\rm m} < h_{\rm m0}$ are stable, neutrally stable and unstable, respectively, where $h_{\rm m0}$ is given by (2.20). Figure 13 also includes the solutions for $h_{\rm m}$ for $\bar{Q} = -5, \ldots, 5$ (i.e. exactly the same solutions as those shown in Figure 12) in order to indicate which are stable and which are unstable.

6. Rivulet Splitting

Having investigated the quasi-steady stability of the present rivulet solutions to small perturbations in Section 5, in this section we determine the conditions under which it is energetically favourable for them to split into subrivulets. In particular, we extend and generalise the recent work of Wilson and Duffy (**19**, **27**) to determine when it is energetically favourable for a rivulet of perfectly wetting fluid on an inclined substrate subject to a prescribed longitudinal surface shear stress to split into one or more subrivulets.

Following the approach of previous authors who investigated sheet break-up and rivulet splitting, and, in particular, that of Schmuki and Laso (**15**), Myers et al. (**18**) and Wilson and Duffy (**19**, **27**) who investigated rivulet splitting, we take the total energy of a rivulet to be the sum of its kinetic and surface energies. If we non-dimensionalise energy per unit

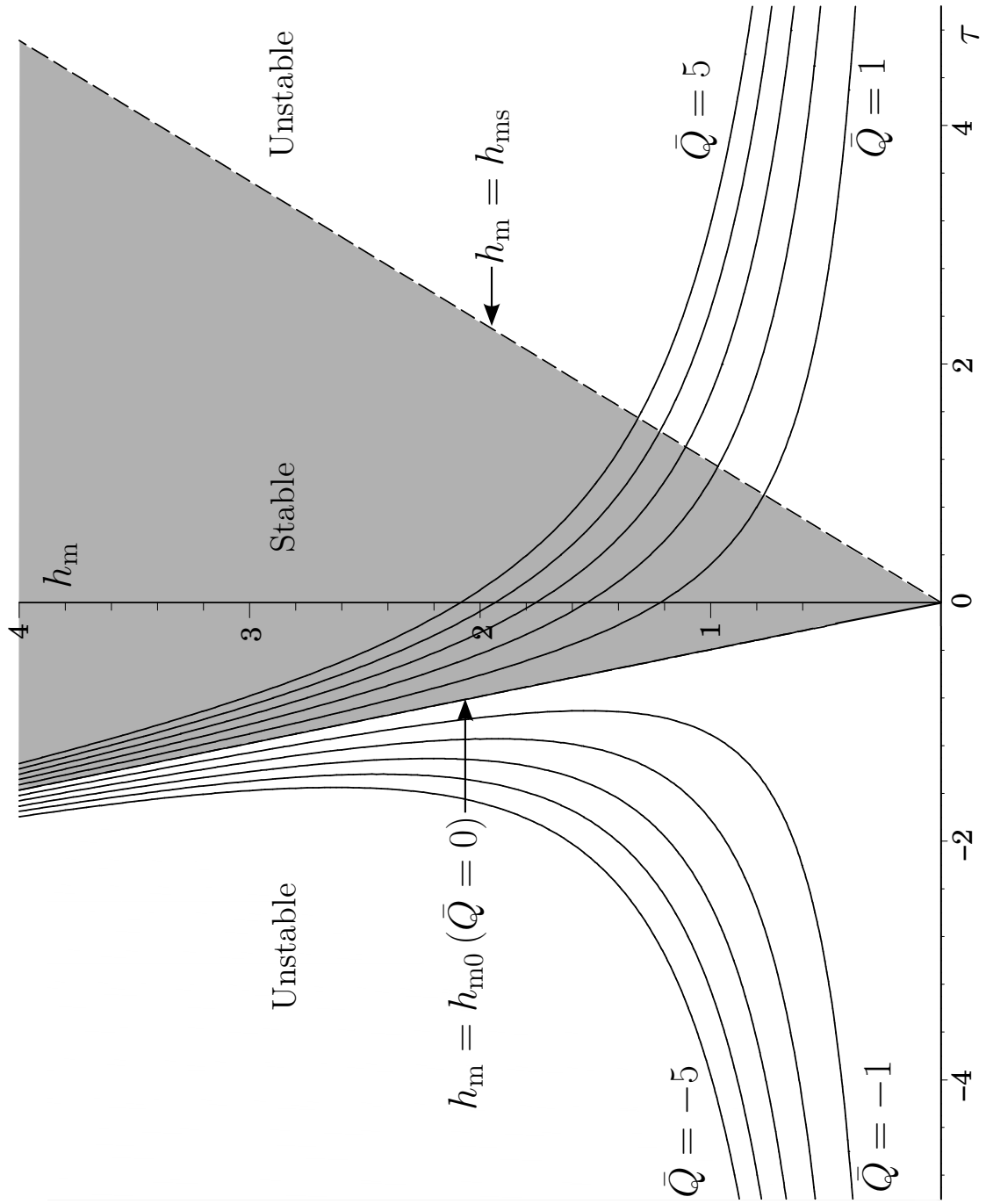

Fig. 13 Plot of the τ–$h_{\rm m}$ parameter plane divided into stable (shaded) and unstable (unshaded) regions according to the quasi-steady stability analysis described in Section 5. Also included are the solutions for $h_{\rm m}$ for $\bar{Q} = -5, \ldots, 5$.

length with $\rho U^2 \epsilon l^2 = \rho^3 g^2 \epsilon^5 l^6/\mu^2$ then the kinetic energy per unit length of a rivulet is given by

$$\frac{1}{2}\int_{-a}^{+a}\int_{0}^{h} u^2(y,z)\,\mathrm{d}z\,\mathrm{d}y, \tag{6.1}$$

and the surface energy per unit length of a rivulet, or, more precisely, the difference between the surface energy of a rivulet and the surface energy of the same width of dry substrate per unit length, is given by

$$\frac{1}{\epsilon^2 W}\left[\int_{-a}^{+a}\left(1+\epsilon^2 h'^2\right)^{\frac{1}{2}}\,\mathrm{d}y - 2a\right], \tag{6.2}$$

where

$$W = \frac{\rho l U^2}{\gamma\epsilon} = \frac{\gamma^2\epsilon^3}{gl\mu^2} \tag{6.3}$$

is an appropriately defined Weber number. Thus, the leading-order expression for the total energy per unit length of a rivulet, E, is given by

$$E = \frac{1}{120}\int_{-a}^{+a}\left(8h^2\sin^2\alpha + 25\tau h\sin\alpha + 20\tau^2\right)h^3\,\mathrm{d}y + \frac{1}{2W}\int_{-a}^{+a} h'^2\,\mathrm{d}y, \tag{6.4}$$

which can be evaluated to give

$$E = \frac{\pi}{7680m}\left(252h_{\mathrm{m}}^2\sin^2\alpha + 875\tau h_{\mathrm{m}}\sin\alpha + 800\tau^2\right)h_{\mathrm{m}}^3 + \frac{m\pi}{8W}h_{\mathrm{m}}^2. \tag{6.5}$$

In the special case $\tau = 0$ equation (6.5) reduces to the corresponding expression obtained by Wilson and Duffy (**27**) for a purely gravity-driven rivulet of perfectly wetting fluid.

Before proceeding any further it is convenient to scale α and W out of the problem by writing

$$\begin{gathered}\tau = \left(\frac{m^2\sin\alpha}{W}\right)^{\frac{1}{3}}\hat{\tau}, \quad h_{\mathrm{m}} = \left(\frac{m^2}{W\sin^2\alpha}\right)^{\frac{1}{3}}\hat{h}_{\mathrm{m}},\\ E = \left(\frac{m^7}{W^5\sin^4\alpha}\right)^{\frac{1}{3}}\hat{E}, \quad Q = \frac{m}{W\sin\alpha}\hat{Q},\end{gathered} \tag{6.6}$$

and to drop the hats in the remainder of this section for clarity to give simplified expressions for the flux (2.17), namely

$$Q = \frac{\pi}{24}\left(5h_{\mathrm{m}} + 9\tau\right)h_{\mathrm{m}}^2 \tag{6.7}$$

and the total energy (6.5), namely

$$E = \frac{\pi}{7680}\left(252h_{\mathrm{m}}^3 + 875\tau h_{\mathrm{m}}^2 + 800\tau^2 h_{\mathrm{m}} + 960\right)h_{\mathrm{m}}^2. \tag{6.8}$$

We shall consider two specific problems concerning the splitting of a rivulet, namely splitting into two, in general, non-identical subrivulets, and splitting into n ($n = 1, 2, 3, \dots$) identical subrivulets.

It is energetically favourable for a rivulet with maximum height h_{m} and flux $\bar{Q}$ to split into two subrivulets, one with maximum height $h_{\mathrm{m}\lambda}$ and flux $\lambda\bar{Q}$ and the other with maximum

height $h_{\mathrm{m}(1-\lambda)}$ and flux $(1-\lambda)\bar{Q}$, where, by conservation of mass, $h_{\mathrm{m}\lambda}$ and $h_{\mathrm{m}(1-\lambda)}$ are related by

$$(5h_{\mathrm{m}}+9\tau)h_{\mathrm{m}}^2=(5h_{\mathrm{m}\lambda}+9\tau)h_{\mathrm{m}\lambda}^2+(5h_{\mathrm{m}(1-\lambda)}+9\tau)h_{\mathrm{m}(1-\lambda)}^2, \tag{6.9}$$

when the difference between the energies of the two states, ΔE, defined by

$$\Delta E=E-\left[E(h_{\mathrm{m}}=h_{\mathrm{m}\lambda})+E(h_{\mathrm{m}}=h_{\mathrm{m}(1-\lambda)})\right], \tag{6.10}$$

is positive. If there is a range of energetically favourable values of λ then the *most* energetically favourable state is the one with the lowest energy and hence the *largest* positive value of ΔE.

Similarly, it is energetically favourable for a rivulet of maximum height h_{m} and flux $\bar{Q}$ to split into n ($n=1,2,3,\dots$) identical subrivulets each of maximum height $h_{\mathrm{m}n}$ and flux $\bar{Q}/n$, where, by conservation of mass, h_{m} and $h_{\mathrm{m}n}$ are related by

$$(5h_{\mathrm{m}}+9\tau)h_{\mathrm{m}}^2=n(5h_{\mathrm{m}n}+9\tau)h_{\mathrm{m}n}^2, \tag{6.11}$$

when the difference between the energies of the two states, ΔE_n, defined by

$$\Delta E_n=E-nE(h_{\mathrm{m}}=h_{\mathrm{m}n}), \tag{6.12}$$

is positive. If there is more than one energetically favourable state then the *most* energetically favourable state is the one with the lowest energy and hence the *largest* positive value of ΔE_n. A state with n subrivulets has the same energy as a state with $n+1$ subrivulets when the difference between the energies of the two states, $\Delta E_{n,n+1}$, defined by

$$\Delta E_{n,n+1}=\Delta E_{n+1}-\Delta E_n, \tag{6.13}$$

is zero.

6.1 *Purely Gravity-Driven Rivulet*

Wilson and Duffy (**27**) examined the case of a purely gravity-driven rivulet (i.e. the case $\tau=0$) for which, from (2.18), $h_{\mathrm{m}}=(24\bar{Q}/5\pi)^{\frac{1}{3}}$, so that from (6.10) the energy difference ΔE is given by

$$\Delta E=\frac{21\pi}{640}\left(\frac{24\bar{Q}}{5\pi}\right)^{\frac{5}{3}}\left[1-\lambda^{\frac{5}{3}}-(1-\lambda)^{\frac{5}{3}}+\frac{50\pi}{63\bar{Q}}\left\{1-\lambda^{\frac{2}{3}}-(1-\lambda)^{\frac{2}{3}}\right\}\right], \tag{6.14}$$

where λ must lie in the interval $0\le\lambda\le1$. In this case $\Delta E<0$ for all $0<\lambda<1$ when $h_{\mathrm{m}}<h_{\mathrm{mc}}(2)$, $\Delta E=0$ at $\lambda=1/2$ when $h_{\mathrm{m}}=h_{\mathrm{mc}}(2)$, and ΔE has a positive global maximum at $\lambda=1/2$ when $h_{\mathrm{m}}>h_{\mathrm{mc}}(2)$, where

$$h_{\mathrm{mc}}(2)=\left[\frac{80(2^{\frac{1}{3}}-1)}{21(1-2^{-\frac{2}{3}})}\right]^{\frac{1}{3}}\simeq1.3883. \tag{6.15}$$

Hence it is energetically favourable for a rivulet to split into two subrivulets when $h_{\mathrm{m}}>h_{\mathrm{mc}}(2)$, and when this condition holds it is always most energetically favourable for the rivulet to split into identical subrivulets each with half the flux of the original rivulet. This

critical value of $h_{\rm m}$ is equivalent to the corresponding critical value of W obtained by Wilson and Duffy (**27**, equation 10). Similarly, from (6.12) the corresponding expression for the energy difference ΔE_n is

$$\Delta E_n = \frac{21\pi}{640}\left(\frac{24\bar{Q}}{5\pi}\right)^{\frac{5}{3}}\left[1 - n^{-\frac{2}{3}} + \frac{50\pi}{63\bar{Q}}\left\{1 - n^{\frac{1}{3}}\right\}\right] \tag{6.16}$$

so that $\Delta E_n = 0$ when $h_{\rm m} = h_{\rm mc}(n)$, where

$$h_{\rm mc}(n) = \left[\frac{80(n^{\frac{1}{3}} - 1)}{21(1 - n^{-\frac{2}{3}})}\right]^{\frac{1}{3}}. \tag{6.17}$$

Hence it is energetically favourable for a rivulet to split into n ($n = 2, 3, 4, \dots$) identical subrivulets when $h_{\rm m} > h_{\rm mc}(n)$. The condition $\Delta E_{n,n+1} = 0$, where $\Delta E_{n,n+1}$ is given by (6.13), yields the critical value of $h_{\rm m}$ at which the most energetically favourable state switches from one with n subrivulets to one with $n + 1$ subrivulets. Hence the most energetically favourable state is the original rivulet (i.e. $n = 1$) for $0 < h_{\rm m} < h_{\rm mc1}$, the two-subrivulet (i.e. $n = 2$) state for $h_{\rm mc1} < h_{\rm m} < h_{\rm mc2}$, the three-subrivulet (i.e. $n = 3$) state for $h_{\rm mc2} < h_{\rm m} < h_{\rm mc3}$, and so on, where

$$h_{{\rm mc}n} = \left[\frac{80\left\{(n+1)^{\frac{1}{3}} - n^{\frac{1}{3}}\right\}}{21\left\{n^{-\frac{2}{3}} - (n+1)^{-\frac{2}{3}}\right\}}\right]^{\frac{1}{3}}. \tag{6.18}$$

This critical value of $h_{\rm m}$ is equivalent to the corresponding critical value of W obtained by Wilson and Duffy (**27**, equation 12). Note that $h_{\rm mc1} = h_{\rm mc}(2)$.

6.2 *Purely Shear-Driven Rivulet*

Also of interest is the case of a purely shear-driven rivulet (i.e. the leading order solution in the limit $|\tau| \to \infty$) for which, from (2.21), $h_{\rm m} = (8\bar{Q}/3\pi\tau)^{1/2}$, so that from (6.10) the energy difference ΔE is given by

$$\Delta E = \left(\frac{50\tau\bar{Q}^3}{243\pi}\right)^{\frac{1}{2}}\left[1 - \lambda^{\frac{3}{2}} - (1-\lambda)^{\frac{3}{2}}\right], \tag{6.19}$$

where λ must again lie in the interval $0 \le \lambda \le 1$. In this case, whatever the value of $h_{\rm m}$, $\Delta E > 0$ for all $0 < \lambda < 1$ and ΔE always has a positive global maximum at $\lambda = 1/2$, and so it is *always* energetically favourable for a rivulet to split into two subrivulets and, moreover, it is always most energetically favourable for the rivulet to split into identical subrivulets each with half the flux of the original. Similarly, from (6.12) the corresponding expression for the energy difference ΔE_n is

$$\Delta E_n = \left(\frac{50\tau\bar{Q}^3}{243\pi}\right)^{\frac{1}{2}}(1 - n^{-\frac{1}{2}}), \tag{6.20}$$

and, since $\Delta E_n > 0$ for $n > 1$, it is *always* energetically favourable for a rivulet to split into n ($n = 2, 3, 4, \dots$) identical subrivulets. Moreover, since ΔE_n is a monotonically increasing function of n, the most energetically favourable state is always that with *infinitely many* subrivulets.

6.3 *General Case*

As the results in Subsections 6.1 and 6.2 show, in the special cases of a purely gravity-driven and a purely shear-driven rivulet, when it is energetically favourable for a rivulet to split into two subrivulets, it is always most energetically favourable for the subrivulets to be identical. Thus for simplicity in the general case in which both gravity and shear stress effects are significant treated in this subsection, we shall consider only splitting into n ($n = 1, 2, 3, \dots$) identical subrivulets

Figure 14 summarises all of the key results on rivulet splitting obtained in the present work in the τ–h_m parameter plane. In particular, Figure 14 shows the (shaded) region of the parameter plane bounded by $h_\mathrm{m} = h_\mathrm{m0} = -9\tau/5$ for $\tau < 0$ and the curve $\Delta E_2 = 0$ in which it is unfavourable for a rivulet to split, and that when $\tau \geq \tau_\mathrm{c}$, where $\tau_\mathrm{c} = (2/3)^{\frac{1}{3}} \simeq 0.8736$, and when $h_\mathrm{m} < h_\mathrm{m0}$ (including the curve $h_\mathrm{m} = h_\mathrm{mmin} = -6\tau/5$) for $\tau < 0$ the most energetically favourable state is that with infinitely many subrivulets. The remainder of the parameter plane is divided by the critical curves $\Delta E_n = 0$ for $n = 3, 4, 5, \dots$ (shown with dashed curves) into regions in which the state with n subrivulets is energetically favourable, and by the critical curves $\Delta E_{n,n+1} = 0$ for $n = 2, 3, 4, \dots$ (shown with solid curves) into regions in which the state with n subrivulets is the most energetically favourable.

It is convenient to consider the cases $\bar{Q} \geq 0$ and $\bar{Q} < 0$ separately in what follows.

6.3.1 Non-Negative Flux $\bar{Q} \geq 0$

Examining the energy difference ΔE_n reveals that $\partial \Delta E_n / \partial n > 0$ for all h_m for $n = 2, 3, 4, \dots$ when $\tau > \tau_\mathrm{c}$ but not when $\tau < \tau_\mathrm{c}$. Hence we deduce that when $\tau > \tau_\mathrm{c}$ it is always energetically favourable for a rivulet to split into n ($n = 2, 3, 4, \dots$) subrivulets and, moreover, that the most energetically favourable state is always that with infinitely many subrivulets.

As Figure 14 shows, the behaviour of a rivulet when $\bar{Q} > 0$ for $0 < \tau < \tau_\mathrm{c}$ and when $\bar{Q} \geq 0$ for $\tau \leq 0$ (i.e. $h_\mathrm{m} \geq h_\mathrm{m0}$ for $\tau \leq 0$) is rather more complicated.

To make analytical progress it is convenient to write $h_{\mathrm{m}n}$ in terms of h_m by introducing a new parameter k (> 0) according to

$$h_{\mathrm{m}n} = k h_\mathrm{m}, \tag{6.21}$$

and hence, from (6.11), h_m is given in terms of k by

$$h_\mathrm{m} = -\frac{9\tau(1 - nk^2)}{5(1 - nk^3)} \tag{6.22}$$

which, from (6.12), gives ΔE_n in terms of n and k as

$$\Delta E_n = \frac{81\pi\tau^2(1 - nk^2)^3}{16 \times 10^5 (1 - nk^3)^5} \left[8000(1 - nk^3)^3 - \tau^3 F_n^3\right], \tag{6.23}$$

where we have defined

$$\begin{aligned} F_n^3 &= 12000(1 - nk^3)^3 \\ &+ \frac{189}{5}(1 - nk^2)\left[324(1 - nk^2)(1 - nk^5) - 625(1 - nk^3)(1 - nk^4)\right]. \end{aligned} \tag{6.24}$$

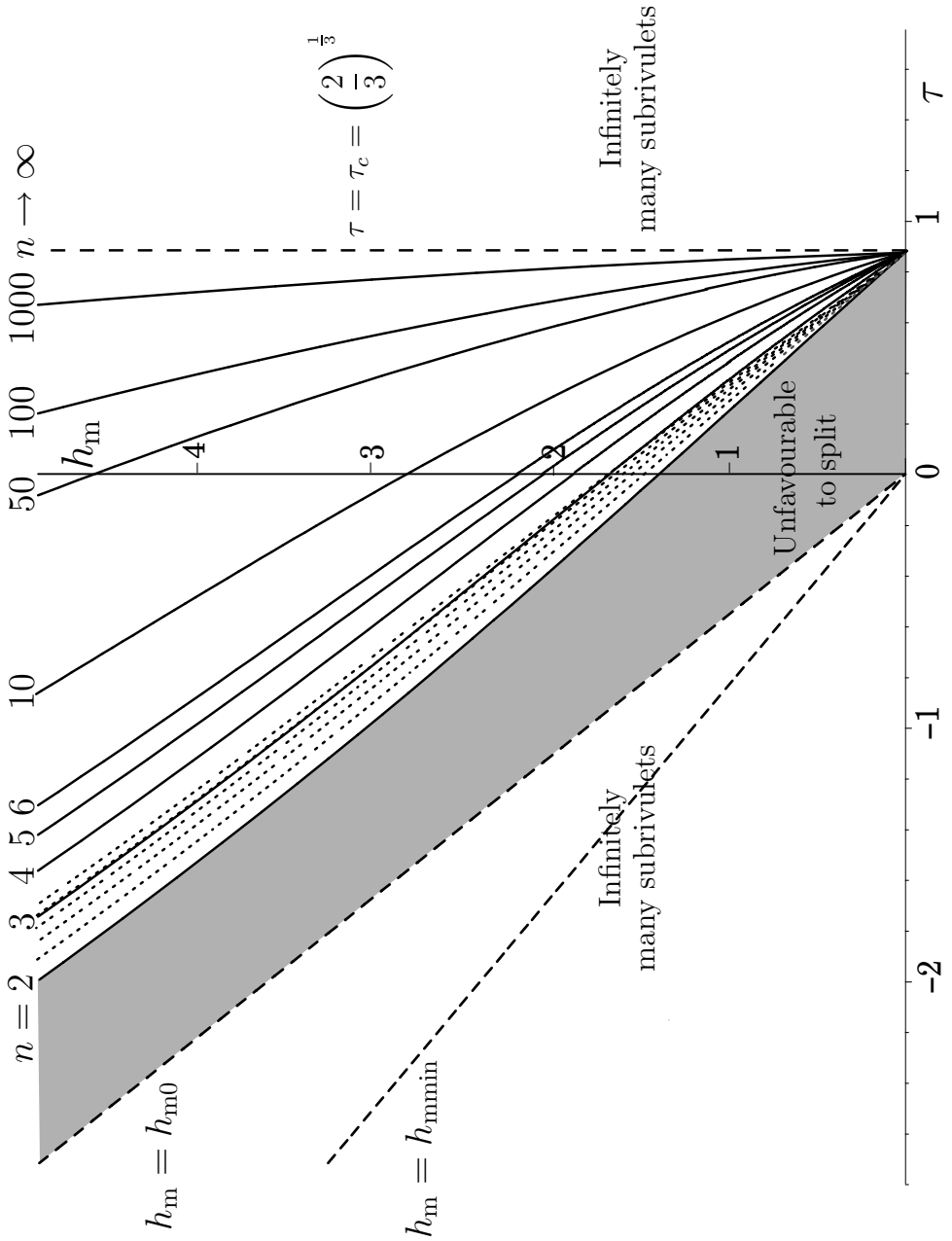

Fig. 14 Plot of the τ–h_m parameter plane showing the (shaded) region bounded by $h_\mathrm{m} = h_{\mathrm{m}0} = -9\tau/5$ for $\tau < 0$ and the curve $\Delta E_2 = 0$ in which it is unfavourable for a rivulet to split, and that when $\tau \geq \tau_\mathrm{c} = (2/3)^{\frac{1}{3}} \simeq 0.8736$ and when $h_\mathrm{m} < h_{\mathrm{m}0}$ (including the curve $h_\mathrm{m} = h_{\mathrm{mmin}} = -6\tau/5$) for $\tau < 0$ the most energetically favourable state is that with infinitely many subrivulets. The remainder of the parameter plane is divided by the critical curves $\Delta E_n = 0$ for $n = 3, 4, 5, \ldots$ (shown with dotted curves) into regions in which the state with n subrivulets is energetically favourable, and by the critical curves $\Delta E_{n,n+1} = 0$ for $n = 2, 3, 4, \ldots$ (shown with solid curves) into regions in which the state with n subrivulets is the most energetically favourable.

From (6.22) and (6.23) the critical curves $\Delta E_n = 0$ have the parametric representation

$$\tau = \frac{20}{F_n}(1 - nk^3), \quad h_{\mathrm{m}} = -\frac{36}{F_n}(1 - nk^2) \tag{6.25}$$

with parameter k. The critical curves $\Delta E_n = 0$ pass through the point $h_{\mathrm{m}} = 0$, $\tau = \tau_{\mathrm{c}}$ (which corresponds to $k = n^{-\frac{1}{2}}$), and intersect $\tau = 0$ (which corresponds to $k = n^{-\frac{1}{3}}$) at $h_{\mathrm{m}} = h_{\mathrm{mc}}(n)$ given by (6.17). In the limit $\tau \to \tau_{\mathrm{c}}^-$ the critical curves $\Delta E_n = 0$ approach $h_{\mathrm{m}} = 0$ linearly in $\tau_{\mathrm{c}} - \tau$ according to

$$h_{\mathrm{m}} \sim \frac{96n^{\frac{1}{2}}(\tau_{\mathrm{c}} - \tau)}{35(n^{\frac{1}{2}} + 1)} \to 0^+. \tag{6.26}$$

In the limit $\tau \to -\infty$ (which corresponds to $k \to k_{\max}(n)^-$, where $k_{\max} = k_{\max}(n)$ is the unique real positive root of $F_n = 0$ for k) the critical curves $\Delta E_n = 0$ become linear in τ according to

$$h_{\mathrm{m}} \sim -\frac{9\tau(1 - nk_{\max}^2)}{5(1 - nk_{\max}^3)} \to \infty, \tag{6.27}$$

and so $k_{\max}(2) \simeq 0.9200$ and $h_{\mathrm{m}} \sim -2.2373\tau$, $k_{\max}(3) \simeq 0.8758$ and $h_{\mathrm{m}} \sim -2.3068\tau$, $k_{\max}(4) \simeq 0.8454$ and $h_{\mathrm{m}} \sim -2.3616\tau$, and $k_{\max}(n) = O(n^{-\frac{1}{5}}) \to 0^+$ and $h_{\mathrm{m}} = -O(n^{\frac{1}{5}})\tau \to \infty$ as $n \to \infty$. The behaviour of the critical curves $\Delta E_n = 0$ in the limit $n \to \infty$ depends on the sign on τ. When $\tau > 0$ the critical curves $\Delta E_n = 0$ approach the finite limiting curve

$$h_{\mathrm{m}} = -\frac{5\left[175\tau^2 - \sqrt{7\tau(3072 - 233\tau^3)}\right]}{504\tau} \tag{6.28}$$

from below as $n \to \infty$. On the other hand, when $\tau \leq 0$ the critical curves $\Delta E_n = 0$ become large like $O(n^{\frac{1}{9}})$ according to

$$h_{\mathrm{m}} \sim \left(\frac{80}{21}\right)^{\frac{1}{3}} n^{\frac{1}{9}} \simeq 1.5618n^{\frac{1}{9}} \to \infty \tag{6.29}$$

when $\tau = 0$ and like $O(n^{\frac{1}{5}})$ according to

$$h_{\mathrm{m}} \sim -\frac{9\tau}{5}\left[\frac{(3111\tau^3 - 40000)n}{61236\tau^3}\right]^{\frac{1}{5}} \to \infty \tag{6.30}$$

when $\tau < 0$ as $n \to \infty$. Details of the relevant calculations are given in Appendix B.

Similarly, it is convenient to write h_{m} in terms of $h_{\mathrm{m}n}$ and $h_{\mathrm{m}(n+1)}$ by defining the new parameters k_n (> 0) and k_{n+1} (> 0) according to

$$h_{\mathrm{m}n} = k_n h_{\mathrm{m}}, \quad h_{\mathrm{m}(n+1)} = k_{n+1} h_{\mathrm{m}} \tag{6.31}$$

and hence, from (6.11), h_{m} is given in terms of k_n and k_{n+1} by

$$h_{\mathrm{m}} = -\frac{9\tau(1 - nk_n^2)}{5(1 - nk_n^3)} = -\frac{9\tau\left\{1 - (n+1)k_{n+1}^2\right\}}{5\left\{1 - (n+1)k_{n+1}^3\right\}} = -\frac{9\tau\left\{(n+1)k_{n+1}^2 - nk_n^2\right\}}{5\left\{(n+1)k_{n+1}^3 - nk_n^3\right\}} \tag{6.32}$$

which, from (6.13), gives $\Delta E_{n,n+1}$ in terms of n, k_n and k_{n+1} as

$$\Delta E_{n,n+1} = \frac{81\pi\tau^2\left\{nk_n^2-(n+1)k_{n+1}^2\right\}^3}{16\times 10^5\left\{nk_n^3-(n+1)k_{n+1}^3\right\}^5}\left[8000\left\{nk_n^3-(n+1)k_{n+1}^3\right\}^3-\tau^3F_{n,n+1}^3\right], \tag{6.33}$$

where we have defined

$$\begin{aligned} F_{n,n+1}^3 &= 12000\left\{nk_n^3-(n+1)k_{n+1}^3\right\}^3 \\ &+\frac{189}{5}\left\{nk_n^2-(n+1)k_{n+1}^2\right\}\Big[324\left\{nk_n^2-(n+1)k_{n+1}^2\right\}\left\{nk_n^5-(n+1)k_{n+1}^5\right\} \\ &-625\left\{nk_n^3-(n+1)k_{n+1}^3\right\}\left\{nk_n^4-(n+1)k_{n+1}^4\right\}\Big]. \end{aligned} \tag{6.34}$$

From (6.32) and (6.33) the critical curves $\Delta E_{n,n+1}=0$ have the parametric representation

$$\tau = \frac{20}{F_{n,n+1}}\left\{nk_n^3-(n+1)k_{n+1}^3\right\}, \quad h_{\rm m} = -\frac{36}{F_{n,n+1}}\left\{nk_n^2-(n+1)k_{n+1}^2\right\} \tag{6.35}$$

with parameters k_n and k_{n+1}. The critical curves $\Delta E_{n,n+1}=0$ pass through the point $h_{\rm m}=0$, $\tau=\tau_{\rm c}$ (which corresponds to $k_n=n^{-\frac{1}{2}}$, $k_{n+1}=(n+1)^{-\frac{1}{2}}$) and intersect $\tau=0$ (which corresponds to $k_n=n^{-\frac{1}{3}}$, $k_{n+1}=(n+1)^{-\frac{1}{3}}$) at $h_{\rm m}=h_{{\rm mc}n}$ given by (6.18). In the limit $\tau\to\tau_{\rm c}^-$, the critical curves $\Delta E_{n,n+1}=0$ approach $h_{\rm m}=0$ linearly in $\tau_{\rm c}-\tau$ according to

$$h_{\rm m}\sim\frac{96n^{\frac{1}{2}}(n+1)^{\frac{1}{2}}(\tau_{\rm c}-\tau)}{35\left\{n^{\frac{1}{2}}+(n+1)^{\frac{1}{2}}\right\}}\to 0^+. \tag{6.36}$$

In the limit $\tau\to-\infty$ (which corresponds to $k_n\to k_{{\rm max}n}^-$ and $k_{n+1}\to k_{{\rm max}(n+1)}^-$, where $k_{{\rm max}n}=k_{{\rm max}n}(n)$ and $k_{{\rm max}(n+1)}=k_{{\rm max}(n+1)}(n)$ are the unique real roots of $F_{n,n+1}=0$ for k_n and k_{n+1} satisfying (6.32)) the critical curves $\Delta E_{n,n+1}=0$ become linear in τ according to

$$h_{\rm m}\sim-\frac{9\tau\left\{(n+1)k_{{\rm max}(n+1)}^2-nk_{{\rm max}n}^2\right\}}{5\left\{(n+1)k_{{\rm max}(n+1)}^3-nk_{{\rm max}n}^3\right\}}\to\infty, \tag{6.37}$$

and so $k_{\rm max1}(1)=1$, $k_{\rm max2}(1)=k_{\rm max}(2)\simeq 0.9200$ and $h_{\rm m}\sim-2.2373\tau$, $k_{\rm max2}(2)\simeq 0.9000$, $k_{\rm max3}(2)\simeq 0.8572$ and $h_{\rm m}\sim-2.4368\tau$, $k_{\rm max3}(3)\simeq 0.8389$, $k_{\rm max4}(3)\simeq 0.8104$ and $h_{\rm m}\sim-2.5941\tau$, and $k_{{\rm max}n}=O(n^{-\frac{1}{3}})\to 0^+$, $k_{{\rm max}(n+1)}=O(n^{-\frac{1}{3}})\to 0^+$ and $h_{\rm m}\sim-O(n^{\frac{1}{3}})\tau\to\infty$ as $n\to\infty$. Unlike for the critical curves $\Delta E_n=0$ described previously, the behaviour of the critical curves $\Delta E_{n,n+1}=0$ in the limit $n\to\infty$ is independent of the sign of τ. For all values of τ the critical curves $\Delta E_{n,n+1}=0$ become large like $O(n^{\frac{1}{3}})$ according to

$$h_{\rm m}\sim-\frac{9\tau(K+1)^{\frac{2}{3}}}{5K}n^{\frac{1}{3}}\to\infty, \tag{6.38}$$

where $K=K(\tau)$ (>-1) is the unique real root of

$$(3111\tau^3-40000)K^3-65583\tau^3K-122472\tau^3=0 \tag{6.39}$$

for $\tau<\tau_{\rm c}$, as $n\to\infty$. Details of the relevant calculations are given in Appendix C.

6.3.2 Negative Flux $\bar{Q} < 0$

As we saw in Section 4, when $Q_{\min} < \bar{Q} < 0$ (and hence necessarily $\tau < 0$) there are two rivulet solutions with the same flux, namely a thick solution satisfying $h_{\mathrm{mmin}} = -6\tau/5 < h_{\mathrm{m}} < h_{\mathrm{m0}}$ and a thin solution satisfying $0 < h_{\mathrm{m}} < h_{\mathrm{mmin}}$, and so there is the possibilility that it may be energetically favourable for the thick rivulet to "split" into the thin one (or vice versa). Since it may be shown that ΔE_1 given by (6.23) is a monotonically decreasing function of k for all $\tau < 0$ satisfying $\Delta E_1 \to 0^-$ as $k \to 1^+$, we deduce that a rivulet with $k < 1$ is always more energetically favourable than a rivulet with the same flux with $k > 1$, i.e. the thin rivulet is *always* more energetically favourable than the corresponding thick rivulet with the same flux. Hence, it is *always* energetically favourable for the thick rivulet to "split" to the corresponding thin rivulet, but it is *never* energetically favourable for the opposite to occur.

All that remains therefore is to consider the splitting of the thin rivulet satisfying $0 < h_{\mathrm{m}} \leq h_{\mathrm{mmin}}$ with $\bar{Q} < 0$ for $\tau < 0$ into n ($n = 2, 3, 4, \ldots$) subrivulets. Since $\Delta E_n > 0$ for $0 < k < n^{-1/2} < 1$ and $\Delta E_n < 0$ for $k > 1$, it is *always* energetically favourable for such a rivulet to split into n identical thinner subrivulets, but it is *never* favourable for it to split into n identical thicker subrivulets. Moreover, since ΔE_n is a monotonically increasing function of n, the most energetically favourable state is always that with infinitely many thin subrivulets. This result is consistent with the behaviour of a purely shear-driven rivulet described in Subsection 6.2.

7. Conclusions

In the present paper we used the lubrication approximation to obtain a complete description of the steady unidirectional flow of a thin rivulet of perfectly wetting fluid on an inclined substrate subject to a prescribed uniform longitudinal surface shear stress.

The possible cross-sectional flow patterns that can occur were categorised into five types which are summarised in Figure 2. When $\tau \geq 0$ the velocity is downwards throughout the rivulet (type I). In contrast, when $\tau < 0$ the velocity can be downwards within the rivulet but is always upwards near the edges of the rivulet. Specifically, the velocity is downwards in the centre of the rivulet when $h_{\mathrm{m}} > h_{\mathrm{V}}$ (types II–IV), but upwards throughout the rivulet when $h_{\mathrm{m}} \leq h_{\mathrm{V}}$ (type V), where h_{V} is given by (3.3).

As Figure 4 shows, the number and nature of rivulet solutions depends on the values of τ, α and $\bar{Q}$. When $\tau \geq 0$ there is one solution when $\bar{Q} > 0$, but no solutions when $\bar{Q} \leq 0$. In contrast, when $\tau < 0$ there is one solution when $\bar{Q} \geq 0$, two solutions when $Q_{\min} < \bar{Q} < 0$ (namely a thick solution satisfying $h_{\mathrm{mmin}} < h_{\mathrm{m}} < h_{\mathrm{m0}}$ and a thin solution satisfying $0 < h_{\mathrm{m}} < h_{\mathrm{mmin}}$), one solution given by $h_{\mathrm{m}} = h_{\mathrm{mmin}}$ when $\bar{Q} = Q_{\min}$, and no solutions when $\bar{Q} < Q_{\min}$, where $Q_{\min}$, h_{mmin} and h_{m0} are given by (4.1) and (2.20), respectively.

Rivulet solutions for varying α (which can be interpreted as describing flow down a slowly varying substrate) and rivulet solutions for varying τ (which can be interpreted as describing flow in the presence of an external airflow exerting a uniform shear stress whose strength varies slowly in time) were analysed and are summarised in Figures 7–11, and Figure 12, respectively.

We investigated the stability of the present rivulet solutions to small perturbations by considering the quasi-steady stability of a pendent rivulet with static contact angle θ_0 (> 0)

in the perfectly wetting limit, $\theta_0 \to 0$, and the results are summarised in Figure 13. In particular, we found that when $\tau > 0$ rivulets with $h_\mathrm{m} \leq h_\mathrm{ms}$ are unstable and rivulets with $h_\mathrm{m} > h_\mathrm{ms}$ are stable, but that when $\tau \leq 0$ rivulets with $h_\mathrm{m} > h_\mathrm{m0}$, $h_\mathrm{m} = h_\mathrm{m0}$ and $h_\mathrm{m} < h_\mathrm{m0}$ are stable, neutrally stable and unstable, respectively, where h_ms is given by (5.11). The full stability problem remains an interesting question for further work.

We also determined the conditions under which it is energetically favourable for the present rivulet solutions to split into one or more subrivulets, and the results are summarised in Figure 14. In the case of a purely gravity-driven rivulet we found that the most energetically favourable state is the original rivulet for $0 < h_\mathrm{m} < h_\mathrm{mc1}$, the two-subrivulet state for $h_\mathrm{mc1} < h_\mathrm{m} < h_\mathrm{mc2}$, the three-subrivulet state for $h_\mathrm{mc2} < h_\mathrm{m} < h_\mathrm{mc3}$, and so on, where, from (6.18), $h_\mathrm{mc}n$ is given by

$$h_\mathrm{mc}n = \left[\frac{80m^2\left\{(n+1)^{\frac{1}{3}} - n^{\frac{1}{3}}\right\}}{21W\sin^2\alpha\left\{n^{-\frac{2}{3}} - (n+1)^{-\frac{2}{3}}\right\}}\right]^{\frac{1}{3}}. \tag{7.1}$$

On the other hand, in the case of a purely shear-driven rivulet we found that the most energetically favourable state is always that with infinitely many subrivulets. In the general case in which both gravity and shear stress effects are significant we found that there is a region of the τ–h_m parameter plane bounded by $h_\mathrm{m} = h_\mathrm{m0}$ for $\tau < 0$ and the curve $\Delta E_2 = 0$ in which it is unfavourable for a rivulet to split, and that when

$$\tau \geq \left(\frac{2m^2\sin\alpha}{3W}\right)^{\frac{1}{3}} \tag{7.2}$$

and when $h_\mathrm{m} < h_\mathrm{m0}$ for $\tau < 0$ the most energetically favourable state is that with infinitely many subrivulets. The remainder of the parameter plane is divided by the critical curves $\Delta E_{n,n+1} = 0$ for $n = 2, 3, 4, \ldots$ into regions in which the state with n subrivulets is the most energetically favourable.

The present work forms part of a larger project on rivulets in the presence of an external airflow, and there are many interesting directions for future work. The present analysis is restricted to the simplest case of steady unidirectional rivulet flow, but (even in the absence of an external air flow) steady rivulet meandering as considered by Le Grand-Piteira, Daerr and Limat (**31**), and fluid braiding as considered by Mertens, Putkaradze and Vorobieff (**32**) are also of considerable interest. It would also be interesting to investigate the effect of a prescribed *transverse* surface shear stress on a rivulet. More generally, the study of more sophisticated models for the effect of an external airflow, such as the non-uniform pressure distribution used by McKinley and Wilson (**6**) and non-uniform longitudinal surface shear stress used by Saber and El-Genk (**17**) or genuinely coupled models such as that used by King and Tuck (**1**) and King et al. (**2**), on a rivulet could be very informative.

Acknowledgements

The first author (JMS) gratefully acknowledges the support of the Engineering and Physical Sciences Research Council via a studentship. All the authors gratefully acknowledge useful discussions with Dr Ian Taylor and his colleagues in the Department of Mechanical Engineering at the University of Strathclyde.

References

1. A. C. King and E. O. Tuck, Thin liquid layers supported by steady air-flow surface traction, *J. Fluid Mech.* **251** (1993) 709–718.

2. A. C. King, E. O. Tuck and J.-M. Vanden-Broeck, Air-blown waves on thin viscous sheets, *Phys. Fluids A* **5** (1993) 973–978.

3. J.-C. Tsao, A. P. Rothmayer and A. I. Ruban, Stability of air flow past thin liquid films on airfoils, *Computers and Fluids* **26** (1997) 427–452.

4. J. J. Kriegsmann, M. J. Miksis and J.-M. Vanden-Broeck, Pressure driven disturbances on a thin viscous film, *Phys. Fluids* **10** (1998) 1249–1255.

5. T. G. Myers and C. P. Thompson, Modeling the flow of water on aircraft in icing conditions, *AIAA Journal* **36** (1998) 1010–1013.

6. I. S. McKinley, S. K. Wilson and B. R. Duffy, Spin coating and air-jet blowing of thin viscous drops, *Phys. Fluids* **11** (1999) 30–47.

7. I. S. McKinley and S. K. Wilson, The linear stability of a ridge of fluid subject to a jet of air, *Phys. Fluids* **13** (2001) 872–883.

8. I. S. McKinley and S. K. Wilson, The linear stability of a drop of fluid during spin coating or subject to a jet of air, *Phys. Fluids* **14** (2002) 133–142.

9. M. Villegas-Díaz, H. Power and D. S. Riley, On the stability of rimming flows to two-dimensional disturbances, *Fluid Dyn. Res.* **33** (2003) 141–172.

10. D. E. Hartley and W. Murgatroyd, Criteria for the break-up of thin liquid layers flowing isothermally over solid surfaces, *Int. J. Heat Mass Transfer* **7** (1964) 1003–1015.

11. T. Hobler, Minimum surface wetting, *Chemia Stosowana* **2B** (1964) 145–159 (in Polish).

12. S. G. Bankoff, Minimum thickness of a draining liquid film, *Int. J. Heat Mass Transfer* **14** (1971) 2143–2146.

13. J. Mikielewicz and J. R. Moszynski, Minimum thickness of a liquid film flowing vertically down a solid surface, *Int. J. Heat Mass Transfer* **19** (1976) 771–776.

14. J. Mikielewicz and J. R. Moszynski, An improved analysis of breakdown of thin liquid films, *Archives of Mechanics* **30** (1978) 489–500.

15. P. Schmuki and M. Laso, On the stability of rivulet flow, *J. Fluid Mech.* **215** (1990) 125–143.

16. M. S. El-Genk and H. H. Saber, Minimum thickness of a flowing down liquid film on a vertical surface, *Int. J. Heat Mass Transfer* **44** (2001) 2809–2825.

17. H. H. Saber and M. S. El-Genk, On the breakup of a thin liquid film subject to interfacial shear, *J. Fluid Mech.* **500** (2004) 113–133.

18. T. G. Myers, H. X. Liang, and B. Wetton, The stability and flow of a rivulet driven by interfacial shear and gravity, *Int. J. Non-Linear Mech.* **39** (2004) 1239–1249.

19. S. K. Wilson and B. R. Duffy, Unidirectional flow of a thin rivulet on a vertical substrate subject to a prescribed uniform shear stress at its free surface, *Phys. Fluids* **17** (2005) 108105-1–108105-4.

20. Y. Hikami and N. Shiraishi, Rain-wind induced vibrations of cables in cable-stayed bridges, *J. Wind Eng. Ind. Aerodyn.* **29** (1988) 409–418.

21. C. Geurts, T. Vrouwenvelder, P. van Staalduinen and J. Reusink, Numerical modelling of rain-wind-induced vibration: Erasmus Bridge, Rotterdam, *Struct. Eng. Int.* **8** (1998) 129–135.

22. Y. L. Xu and L. Y. Wang, Analytical study of wind-rain-induced cable vibration: SDOF

model, *J. Wind Eng. and Ind. Aerodyn.* **91** (2003) 27–40.
23. C. Lemaitre, M. Mahmud Alam, P. Hémon, E. de Langre and Y. Zhou, Rainwater rivulets on a cable subject to wind, *C. R. Mécanique* **334** (2006) 158–163.
24. P. A. Kuibin, An asymptotic description of the rivulet flow along an inclined cylinder, *Russ. J. Engng. Thermophys.* **6** (1996) 33–45.
25. S. V. Alekseenko, P. I. Geshev and P. A. Kuibin, Free-boundary fluid flow on an inclined cylinder, *Soviet Phys. Dokl.* **42** (1997) 269–272. Translated from *Dokl. Akad. Nauk.* **354** (1997) 47–50 (in Russian).
26. S. K. Wilson and B. R. Duffy, A rivulet of perfectly wetting fluid draining steadily down a slowly varying substrate, *IMA J. Appl. Math.* **70** (2005) 293–322.
27. S. K. Wilson and B. R. Duffy, When is it energetically favorable for a rivulet of perfectly wetting fluid to split?, *Phys. Fluids* **17** (2005) 078104-1–078104-3.
28. H. K. Moffatt, Behaviour of a viscous film on the outer surface of a rotating cylinder, *J. Mécanique* **16** (1977) 651–673.
29. S. K. Wilson, R. Hunt and B. R. Duffy, On the critical solutions in coating and rimming flow on a uniformly rotating horizontal cylinder, *Q. J. Mech. Appl. Math.* **55** (2002) 357–383.
30. S. K. Wilson and B. R. Duffy, On the gravity-driven draining of a rivulet of viscous fluid down a slowly varying substrate with variation transverse to the direction of flow, *Phys. Fluids* **10** (1998) 13–22.
31. N. Le Grand-Piteira, A. Daerr and L. Limat, Meandering rivulets on a plane: a simple balance between inertia and capillarity?, *Phys. Rev. Lett.* **96** (2006) 254503-1–254503-4.
32. K. Mertens, V. Putkaradze and P. Vorobieff, Morphology of a stream flowing down an inclined plane. Part 1. Braiding, *J. Fluid Mech.* **531** (2005) 49–58.

APPENDIX A

Real Positive Solutions of Equation (2.19) in the General Case $\tau \neq 0$

In this Appendix we present the real positive solutions $h_{\rm m}$ of the cubic polynomial equation (2.19), namely

$$\left(\frac{h_{\rm m}\sin\alpha}{\tau}\right)^3 + \frac{9}{5}\left(\frac{h_{\rm m}\sin\alpha}{\tau}\right)^2 = \frac{24\bar{Q}m\sin^2\alpha}{5\pi\tau^3}, \tag{A.1}$$

in the general case $\tau \neq 0$.

One may show that when $0 \leq \bar{Q}m\sin^2\alpha/\tau^3 \leq 9\pi/50$ and $\tau > 0$ there is a unique solution

$$h_{\rm m} = \frac{6\tau}{5\sin\alpha}\left[-\frac{1}{2} + \cos\phi\right], \tag{A.2}$$

that when $0 \leq \bar{Q}m\sin^2\alpha/\tau^3 \leq 9\pi/50$ and $\tau < 0$ there are two solutions, namely a "thin" solution

$$h_{\rm m} = \frac{6\tau}{5\sin\alpha}\left[-\frac{1}{2} + \cos\left(\frac{2}{3}\pi - \phi\right)\right] \tag{A.3}$$

and a "thick" solution

$$h_{\rm m} = \frac{6\tau}{5\sin\alpha}\left[-\frac{1}{2} + \cos\left(\frac{2}{3}\pi + \phi\right)\right], \tag{A.4}$$

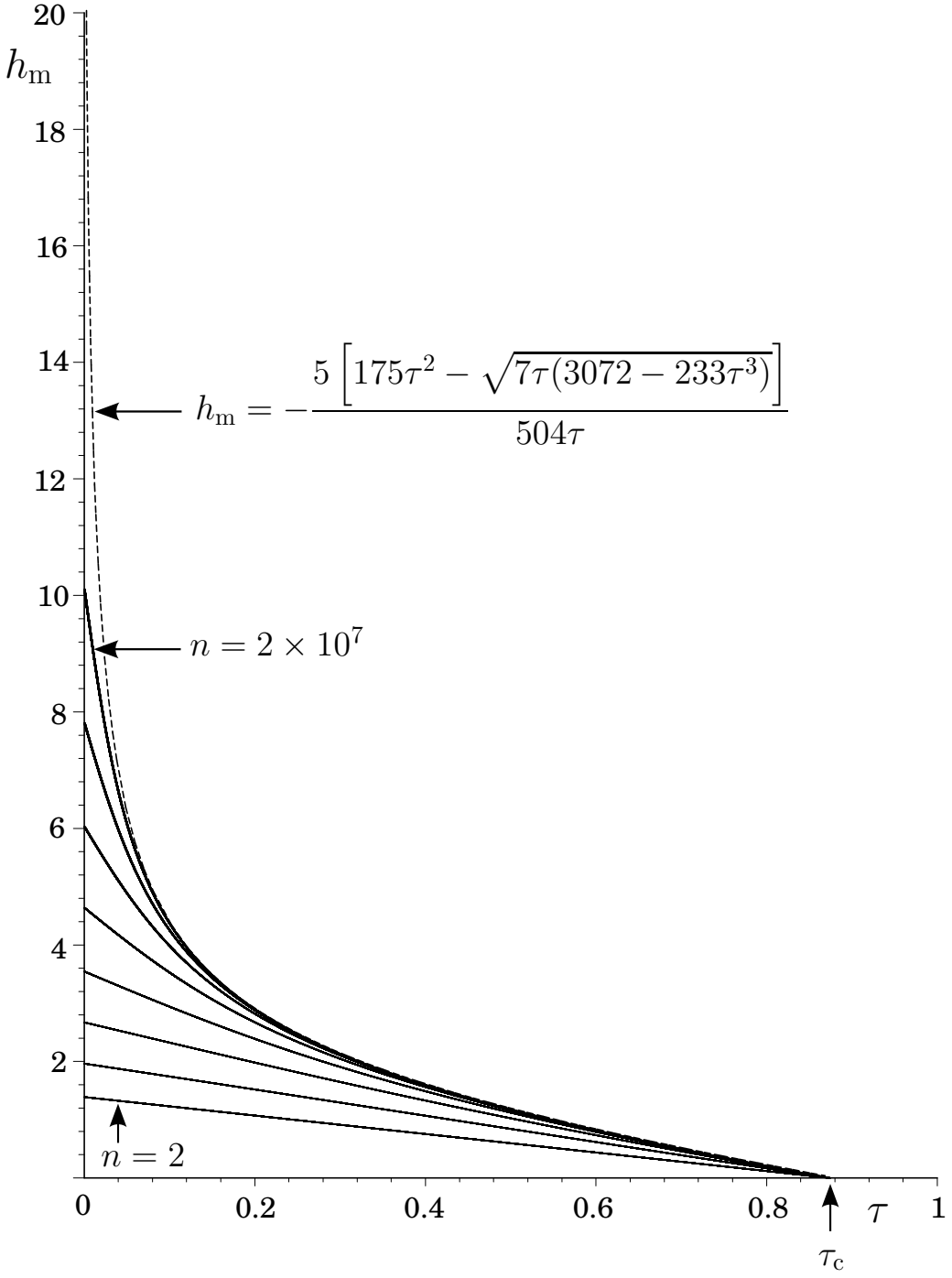

Fig. 15 Plot of the critical curves $\Delta E_n = 0$ for $\tau > 0$ for $n = 2, 20, 200, \ldots, 2 \times 10^7$ (shown with solid curves) and the finite limiting curve $\Delta E_n = 0$ in the limit $n \to \infty$ given by (B.3) (shown with a dashed curve).

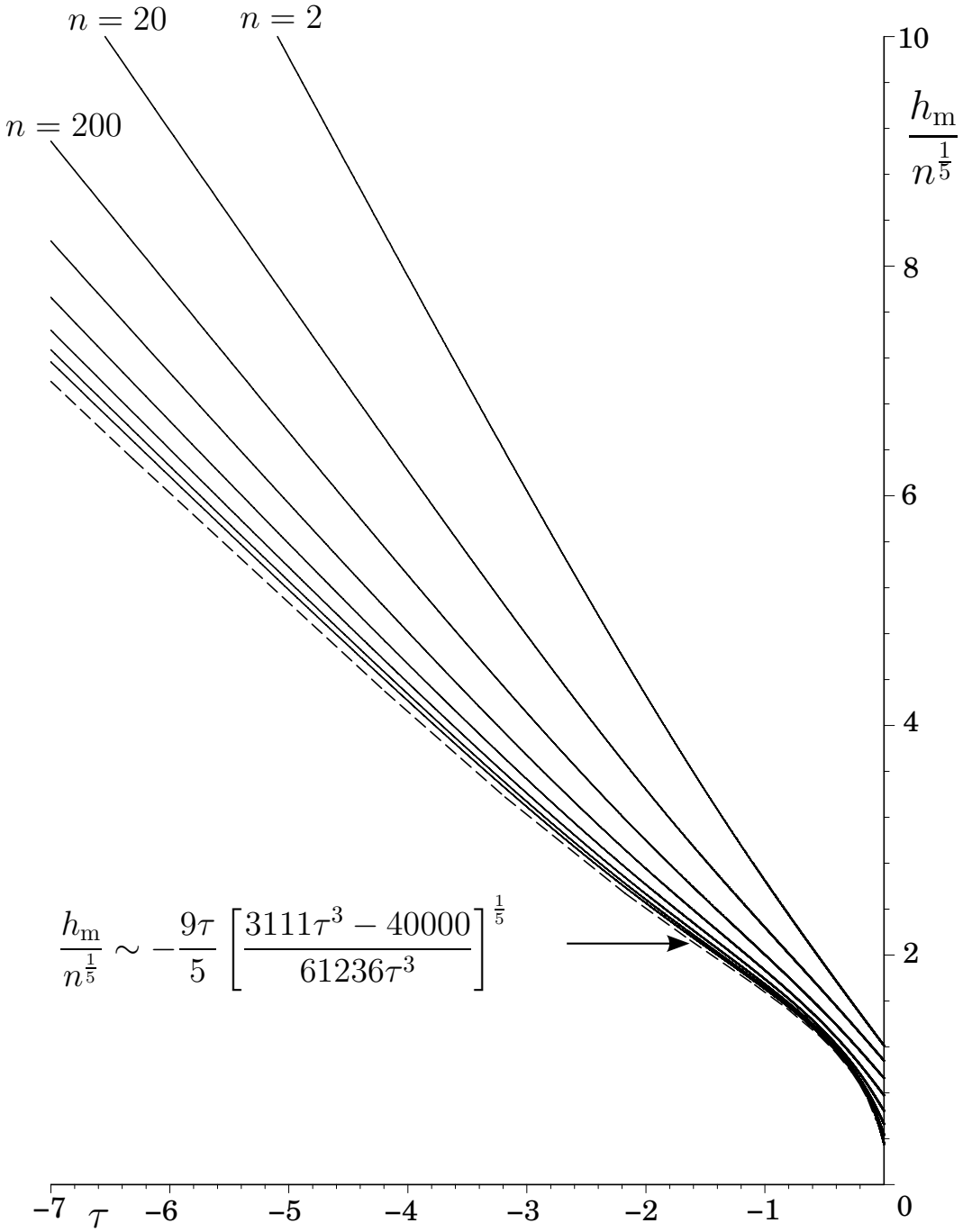

Fig. 16 Plot of the scaled critical curves $\Delta E_n = 0$ for $\tau < 0$ for $n = 2, 20, 200, \ldots, 2 \times 10^7$ (shown with solid curves) and the limiting curve $\Delta E_n = 0$ in the limit $n \to \infty$ given by (B.9) (shown with a dashed curve).

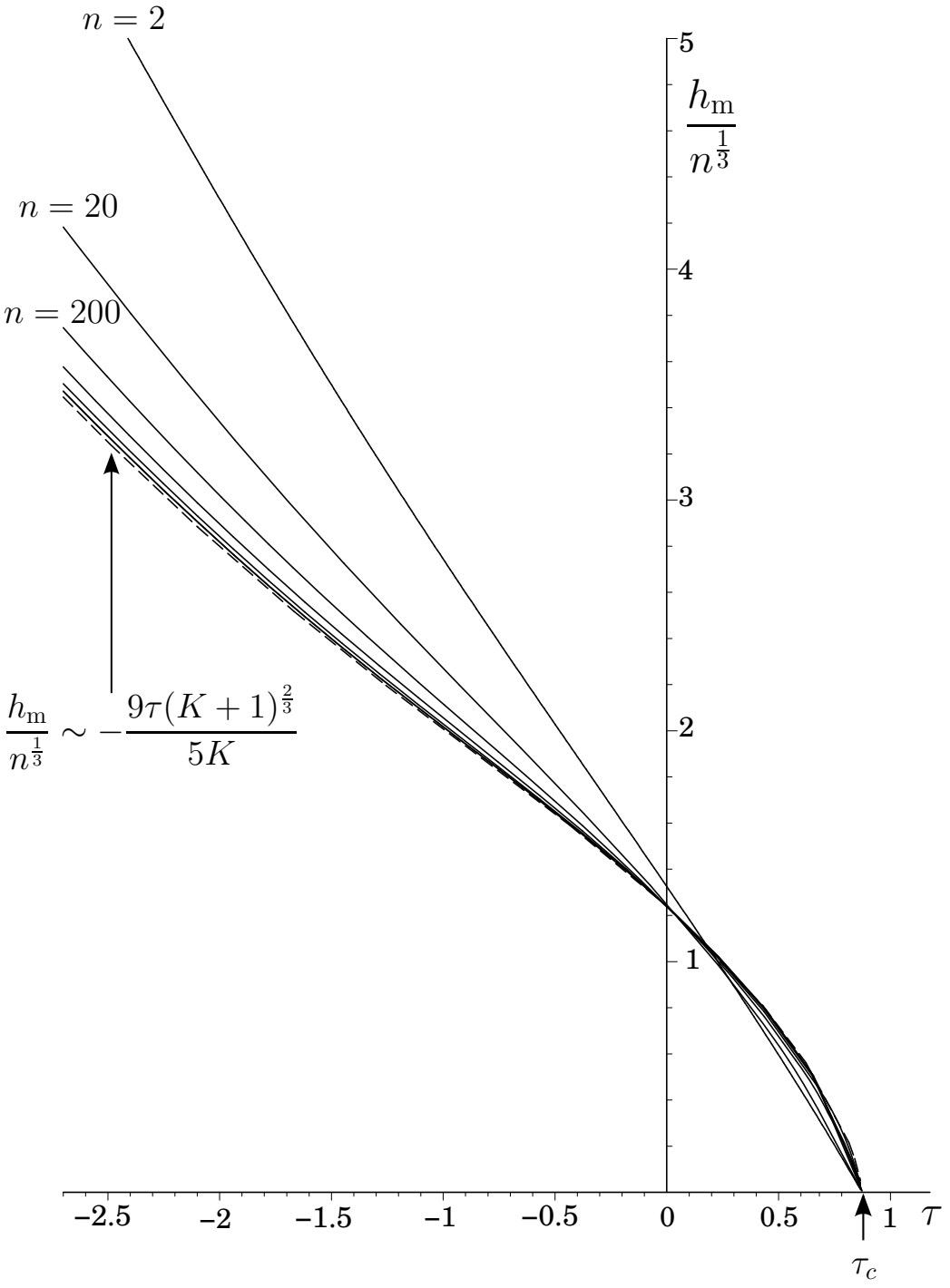

Fig. 17 Plot of the scaled critical curves $\Delta E_{n,n+1} = 0$ for $n = 2, 20, 200, \ldots, 2 \times 10^5$ (shown with solid curves) and the limiting curve $\Delta E_{n,n+1} = 0$ in the limit $n \to \infty$ given by (C.4) (shown with a dashed curve).

and that when $\bar{Q}m\sin^2\alpha/\tau^3 < 0$ for $\tau < 0$ or $\bar{Q}m\sin^2\alpha/\tau^3 > 9\pi/50$ for $\tau > 0$ there is a unique solution

$$h_{\rm m} = \frac{6\tau}{5\sin\alpha}\left[-\frac{1}{2} + \mathrm{sgn}(K)\cosh\left(\frac{1}{3}\cosh^{-1}|K|\right)\right], \tag{A.5}$$

where

$$\phi = \frac{1}{3}\cos^{-1}K \tag{A.6}$$

and

$$K = \frac{100\bar{Q}m\sin^2\alpha}{9\pi\tau^3} - 1. \tag{A.7}$$

APPENDIX B

Asymptotic Behaviour of the Critical Curves $\Delta E_n = 0$ in the Limit $n \to \infty$

In this Appendix we determine the asymptotic behaviour of the critical curves $\Delta E_n = 0$ in the limit $n \to \infty$. The behaviour depends on the sign of τ, and so the cases $\tau > 0$, $\tau = 0$ and $\tau < 0$ are treated separately.

B.1 $\tau > 0$

When $\tau > 0$ we find from (6.25) that $k = O(n^{-\frac{1}{2}}) \to 0^+$ and $h_{\rm m} = O(1)$ as $n \to \infty$, and so we write

$$k \sim k_0 n^{-\frac{1}{2}}, \quad h_{\rm m} \sim -\frac{9\tau(1-k_0^2)}{5}. \tag{B.1}$$

Substituting these expressions into $\Delta E_n = 0$ reveals that

$$k_0^2 = \frac{161\tau^2 + 25\sqrt{7\tau(3072 - 233\tau^3)}}{4536\tau^2}, \tag{B.2}$$

and hence

$$h_{\rm m} \sim -\frac{5\left[175\tau^2 - \sqrt{7\tau(3072-233\tau^3)}\right]}{504\tau}. \tag{B.3}$$

In particular, (B.3) gives

$$h_{\rm m} \sim \frac{96(\tau_{\rm c} - \tau)}{35} \to 0^+ \tag{B.4}$$

as $\tau \to \tau_{\rm c}^-$, and

$$h_{\rm m} \sim \frac{20}{63}\left(\frac{21}{\tau}\right)^{\frac{1}{2}} \simeq 1.4548\tau^{-\frac{1}{2}} \to \infty \tag{B.5}$$

as $\tau \to 0^+$. Figure 15 shows how the critical curves $\Delta E_n = 0$ for $\tau > 0$ for $n = 2, 20, 200, \ldots, 2\times10^7$ (shown with solid curves) approach the finite limiting curve (B.3) (shown with a dashed curve) as n increases.

B.2 $\tau = 0$

When $\tau = 0$ we find $h_{\rm m} = h_{\rm mc}(n)$, where $h_{\rm mc}(n)$ is given by (6.17), and so

$$h_{\rm m} \sim \left(\frac{80}{21}\right)^{\frac{1}{3}} n^{\frac{1}{9}} \simeq 1.5618 n^{\frac{1}{9}} \to \infty. \tag{B.6}$$

B.3 $\tau < 0$

When $\tau < 0$ we find from (6.25) that $k = O(n^{-\frac{1}{5}}) \to 0^+$ and $h_\mathrm{m} = O(n^{\frac{1}{5}}) \to \infty$ as $n \to \infty$, and so we write

$$k \sim k_0 n^{-\frac{1}{5}}, \quad h_\mathrm{m} \sim -\frac{9\tau n^{\frac{1}{5}}}{5k_0}. \tag{B.7}$$

Substituting these expressions into $\Delta E_n = 0$ reveals that

$$k_0^5 = \frac{61236\tau^3}{3111\tau^3 - 40000}, \tag{B.8}$$

and hence

$$h_\mathrm{m} \sim -\frac{9\tau}{5}\left[\frac{(3111\tau^3 - 40000)n}{61236\tau^3}\right]^{\frac{1}{5}}. \tag{B.9}$$

In particular, (B.9) gives

$$\frac{h_\mathrm{m}}{n^{\frac{1}{5}}} \sim \frac{9}{5}\left(\frac{10000}{15309}\right)^{\frac{1}{5}}(-\tau)^{\frac{2}{5}} \simeq 1.6530(-\tau)^{\frac{2}{5}} \to 0^+ \tag{B.10}$$

as $\tau \to 0^-$, and

$$\frac{h_\mathrm{m}}{n^{\frac{1}{5}}} \sim -\frac{9}{5}\left(\frac{1037}{20412}\right)^{\frac{1}{5}}\tau \simeq -0.9919\tau \to \infty \tag{B.11}$$

as $\tau \to -\infty$. Figure 16 shows how the scaled critical curves $\Delta E_n = 0$ for $\tau < 0$ for $n = 2, 20, 200, \ldots, 2 \times 10^7$ (shown with solid curves) approach the limiting curve (B.9) (shown with a dashed curve) as n increases.

APPENDIX C

Asymptotic Behaviour of the Critical Curves $\Delta E_{n,n+1} = 0$ in the Limit $n \to \infty$

In this Appendix we determine the asymptotic behaviour of the critical curves $\Delta E_{n,n+1} = 0$ in the limit $n \to \infty$.

If we write

$$\begin{aligned} k_n &= c_{11}n^{-\frac{1}{3}} + c_{12}n^{-\frac{2}{3}} + c_{13}n^{-1} + c_{14}n^{-\frac{4}{3}} + O(n^{-\frac{5}{3}}), \\ k_{n+1} &= c_{21}n^{-\frac{1}{3}} + c_{22}n^{-\frac{2}{3}} + c_{23}n^{-1} + c_{24}n^{-\frac{4}{3}} + O(n^{-\frac{5}{3}}) \end{aligned} \tag{C.1}$$

as $n \to \infty$, then the relationships between coefficients c_{1i} and c_{2i} for $i = 1, 2, 3, 4$ are determined by substituting into (6.32) and expanding up to and including $O(n^{-\frac{4}{3}})$. Specifically, we find that $c_{11} = c_{21}$, $c_{12} = c_{22}$ and $c_{13} = c_{23}$, but that

$$c_{24} = c_{14} - \frac{c_{11}}{2 + c_{11}^3} \ (\neq c_{14}). \tag{C.2}$$

Hence substituting the expansions (C.1) into $\Delta E_{n,n+1}$ reveals that

$$\begin{aligned} \Delta E_{n,n+1} \sim -\frac{81\pi\tau^2 c_{11}^9}{8 \times 10^6 (c_{11}^3 + 2)(c_{11}^3 - 1)^5}\Big[&40000(c_{11} - 1)^3(c_{11}^2 + c_{11} + 1) \\ &- (3111c_{11}^9 - 9333c_{11}^6 - 56250c_{11}^3 - 60000)\tau^3\Big] \end{aligned} \tag{C.3}$$

as $n \to \infty$. Note that is necessary to expand k_n and k_{n+1} up to and including $O(n^{-\frac{4}{3}})$ as we have done here in order to obtain the correct leading order behaviour of $\Delta E_{n,n+1}$. Hence, if we write $c_{11}^3 = K + 1$ for simplicity, then the critical curve $\Delta E_{n,n+1} = 0$ is given by

$$h_\mathrm{m} \sim -\frac{9\tau(K+1)^{\frac{2}{3}}n^{\frac{1}{3}}}{5K} \to \infty, \tag{C.4}$$

where $K = K(\tau)$ (> -1) is the unique real root of

$$(3111\tau^3 - 40000)K^3 - 65583\tau^3 K - 122472\tau^3 = 0 \tag{C.5}$$

for $\tau < \tau_{\rm c}$.

In particular, (C.4) gives

$$\frac{h_{\rm m}}{n^{\frac{1}{3}}} \sim \frac{9}{5}\left(\frac{8}{7}\right)^{\frac{2}{3}}\left(\frac{2}{3}\right)^{\frac{7}{9}}(\tau_{\rm c} - \tau)^{\frac{2}{3}} \simeq 1.4354(\tau_{\rm c} - \tau)^{\frac{2}{3}} \to 0^+ \tag{C.6}$$

(corresponding to $K \to -1^+$) as $\tau \to \tau_{\rm c}^-$,

$$\frac{h_{\rm m}}{n^{\frac{1}{3}}} \sim \left(\frac{40}{21}\right)^{\frac{1}{3}} \simeq 1.2396 \tag{C.7}$$

(corresponding to $K \to 0$, and in agreement with the large n limit of $h_{\rm m} = h_{{\rm mc}n}$) as $\tau \to 0$, and

$$\frac{h_{\rm m}}{n^{\frac{1}{3}}} \sim -\frac{9\tau(K+1)^{\frac{2}{3}}n^{\frac{1}{3}}}{5K} \simeq -1.1552\tau \to \infty \tag{C.8}$$

(corresponding to $K \to K_{\rm max}^-$, where $K_{\rm max} \simeq 5.3348$ is the unique real root of $1037K^3 - 21861K - 40824 = 0$ for K) as $\tau \to -\infty$.

Figure 17 shows how the scaled critical curves $\Delta E_{n,n+1} = 0$ for $n = 2, 20, 200, \ldots, 2\times 10^7$ (shown with solid curves) approach the limiting curve (C.4) (shown with a dashed curve) as n increases.